Tissues-on-a-String: Analyzing Transport Within Tissues Via Perfusable Glass-Sheathed Hydrogel Microtubes

A thesis submitted to McGill University in partial fulfillment of the requirements for the degree of Master of Science in Chemical Engineering

Chen Li
Department of Chemical Engineering
McGill University, Montreal

OCTOBER 1, 2022

Abstract

Measuring transport of soluble molecules such as nutrients, waste, and therapeutics within tissues is essential to understand the impact of culture dimensionality on tissue function, and to realize improved 3D cell culture discovery platforms. Studying these properties on conventional 3D cell cultures poses great challenges as the delivering or sampling access within these complex 3D tissue structures is either challenging to precisely position within the desired region or simply destructive. In this thesis, we demonstrate proof-of-concept for a simple technique to both deliver and sample soluble factors from a point source within spheroids, using a highly perfusable hollow-core hydrogel microtube and an integrated glass capillary sheathing system, that successfully limits transport to a well-defined region inside the tissue. We successfully demonstrated its applicability by analyzing the transport properties of a model placental trophoblast choriocarcinoma, cultured as a 3D spheroid. Through comparison with finite element modeling of soluble diffusion in our platform, we found that the diffusivity within placental spheroid is heterogeneous as it shows higher diffusivity towards its core and gradually decreases the edge. This platform provides a simple design that could be used to rapidly study diffusion of soluble within a 3D tissue.

Résumé

La mesure du transport de molécules solubles comme les nutriments, les déchets et les thérapeutiques dans les tissus est essentielle pour comprendre l'impact de la dimensionnalité de la culture cellulaire sur leur fonction et pour fabriquer des nouvelles plate-formes de découverte en 3D. L'étude de ces caractéristiques sur les cultures cellulaires conventionnelles en 3D pose de grands défis car l'accès pour la distribution ou l'échantillonnage dans ces structures tissulaires complexes en 3D est soit difficile à positionner avec précision dans la région souhaitée, soit facilement détruire la culture. Dans cette thèse, nous démontrons la preuve de concept d'une simple technique permettant à la fois de distribuer et d'échantillonner des facteurs solubles à partir d'une point source dans des sphéroïdes cellulaires en utilisant une microtube d'hydrogel à l'âme creuse extrêmement perfusable et un système de tube capillaire agissant comme un fourreau qui limite le transport à une région bien définie à l'intérieur du tissu. Nous avons démontré avec succès son applicabilité en analysant les propriétés de transport d'un modèle de choriocarcinome trophoblastique placentaire, cultivé sous forme de sphéroïde 3D. Par comparaison avec la méthode des éléments finis de la diffusion soluble dans notre plate-forme, nous avons constaté que la diffusivité dans le sphéroïde placentaire est irrégulière, car la diffusivité est plus élevée vers le noyau du sphéroïde et diminue progressivement le bord. Cette plate-forme fournit un simple désign pour les études impliquant un transfert de masse comme nous l'avons démontré avec la formation de sphéroïdes BeWo, mais pourrait également être utilisée pour une variété d'autres cultures cellulaires.

Acknowledgements

It is an understatement when I say that I absolutely enjoyed every moment not just conducting research but just being present and part of Cellular Microenvironment Design lab. It is also an understatement to say that this was primarily all thanks to my supervisor Prof. Christopher Moraes. Chris is a life changing mentor that one can't ask but only wish for. He created a unique research environment full of passion and freedom in which I always felt comfortable letting my creativity go wild and explore the full potential of science and engineering. I'm also grateful for Chris to always have our best interest in mind and looking out after us by giving us amazing opportunities whenever there's chance.

Everyone in our lab is absolutely simply fantastic. We really took the motto of "work hard, play hard" to the next level and I've never felt this amount of synergy and chemistry within such large group before. Thus I would like to take this chance to thank my colleagues individually. To Nick and Camille, thank you both for being my supervisor when I started my research journey. Your help and company were undeniably what set this positive and joyful tone during the takeoff my research journey which I've kept until today. I could always count on Nick's unmatched sense of humor and Camille's life-saving chocolate to make my day. To Ray, thank you for acting like the calm big brother that I could always come to for anything. To Steph, thank you for organizing all the activities together and making the lab more fun. To Nik, thank you for our late-night lab work and chats. To Wontae, thank you for making fun of Nick with me. To Christina, thank you for your baked treats and making sure we didn't die in the lab. To Gabe, thank you for all the magical knowledge on RNAseq that I absorbed through you via reverse osmosis. To Carley, thank you for

the heartful energy you brought to the lab. To Karthick, thank you for all the projects we shared and help I got from you. To James, thank you for starting master's with me and sharing common interests even though we are so different (I still can't forgive you for hating poutine). To Ben and Nick W. (no. 3), thank you for being fun officemates and losing money in stocks with me and specifically to Ben for saving me countless times in process control and to Nick for trusting me in my meme stocks. To Scott, thank you for the amazing food you made at the chalet.

Outside of the lab, I would like to thank all my badminton friends and teammates. The cheerful energy I get from them during competitions, trainings and social events allowed me stay healthy both physically and mentally.

This thesis marks the end of my master's degree but it is only the start of my Ph.D. research journey!

Contributions of Authors

The platform fabrication, data acquirement and analysis were performed entirely by the author, except for finite element modeling of the transport within glass-hydrogel microtube which was contributed by Nikita Kalashnikov and the side experiment on the effect of forskolin on regular BeWo membrane which was contributed by Erdem Cakmak. This work and writing of this thesis were conducted under the supervision of Dr. Christopher Moraes.

The design of the glass-hydrogel microtube component was mainly contributed by the author and Nikita Kalashnikov.

Table of Contents

List of figures

1. Introduction

Cell culture models are one of the most important tools in every biology related research field as it provides the possibility to perform biological studies on models instead of human beings. These models allowed researchers to make critical medical advances in cancer research, stem cell study, drugs and vaccines discoveries. In recent years, the increase in need for cell culture models with high physiological relevancy has driven a transition from the traditional two-dimensional (2D) cell cultures, which mainly involved the culture of cells on flat surfaces such as petri dishes, to 3D cell cultures. 3D cell cultures subject cells in a 3D environment improving the authenticity of cells communication and interaction with each other and the surrounding environment. In addition, realistic concentration gradients of nutrients, oxygen, and other soluble could be established within 3D cell models similar to *in vivo* environments to achieve more physiologically relevant results in studies. In cancer research, their realistic response to stimulants such as drugs makes them increasingly popular as drug screening platform. 3D cell cultures also include the use of miniature artificial organs developed from stem cells which has drastically improved the relevance of *in vitro* studies across the whole field of tissue engineering.

Although all these 3D cell cultures can recreate closely the cellular, functional and structural characteristics of real tissues, the potential types of studies that could be performed on these models are somehow relatively limited due to measuring and sampling challenges posed by the restricted access to different sites of these cell culture models with complex geometry. For instance, even for a simple shaped spherical tissue, measuring the transport process across or within the tissue is essentially impossible; Former due to difficulty of controlling transport strictly

across a 3D shape and latter due to lack of measuring or sampling access within an enclosed restricted spherical aggregate of cells without destructing the integrity of the model. In this thesis, a new 3D cell culture platform was developed to solve these issues. A glass-sheathed hydrogel microtube was engineered within a polyacrylamide (PAAm) pocket to grow a 3D cell culture "wrapped" around a hydrogel string in which the diffusion is controlled. This developed "tissue-on-a-string" platform enables the delivery and sampling access to any 3D cell culture right within its core. This creates an artificial lumen within tissues and could be used in any cell culture studies involving transport.

2. Literature Review

Traditional 2D cell cultures which mainly involves growing cells in petri dishes have been used by scientists for many decades as an initial test model before moving to animal testing. However, it was often shown that cellular behaviors in 2D petri dishes were very different from the tissues or organs in vivo which are in a 3D environment, and this led to misleading results massively hindering research efficiency. It was very apparent that there was a gap between cell cultures grown in labs and animal models in clinical trials. In attempt to bridge this gap, 3D cell cultures have gained tremendous popularity in recent years as it has shown its ability to closely model cells in vivo while being cultured in vitro (Figure 1).[1] It has been shown that 3D cell cultures better mimic native tissues and organs in their gene and protein expression, functionalities, and microscale tissue architecture.[2]

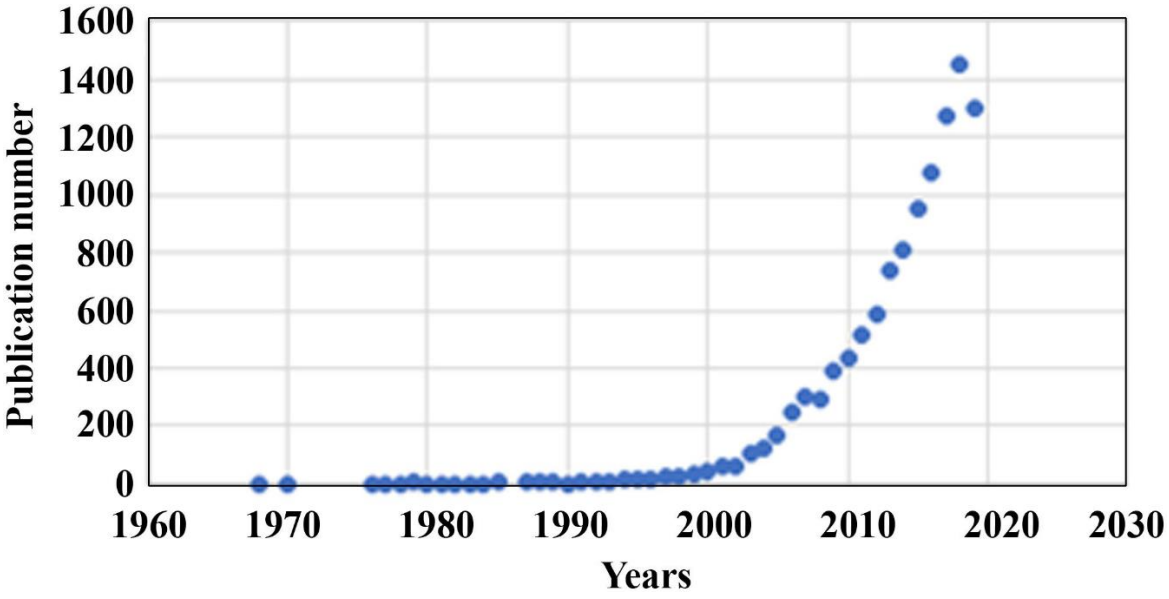

Figure 1. Number of publications per year from 1968 to 2020 on 3D cell cultures from Caleb et al. (Frontiers).[1]

2.1 Spheroids

One of the most common 3D cell culture models are spheroids. Defined as a spherical micro-aggregate of cells, they were initially developed as 3D aggregate of cancer cells to mimic tumors and their response to therapy.[3,4] These 3D spheroids can recreate cellular, functional and structural characteristics of a tissue *in vitro* closer than 2D cell cultures.[5] Due to its simplistic spherical shape, spheroids are very easy to form (formation process shown in Figure 2) even at a high-throughput quantity which made spheroids a popular drug screening platform for cancer therapy.[6–8]

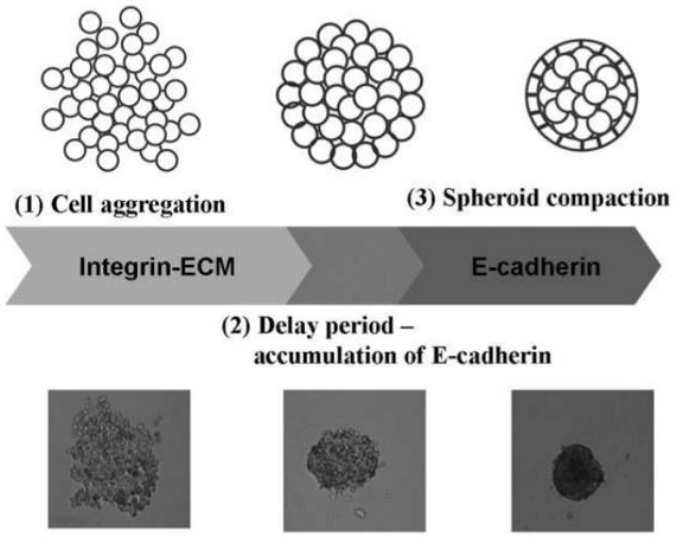

Figure 2. Spheroid formation process.[9]

There have been many spheroids formation techniques developed in the past years and they can be separated into 3 general systems: rotation-based culture systems, well-based systems, and microfluidic systems.[10] Each system also has different spheroid formation techniques which can be further categorized; I will particularly focus on microwells[11,12] from well-based systems and centrifugal forced aggregation technique[13] from rotation-based culture systems as they provided the basic inspirations of the platform developed in this thesis.

2.1.1 Microwells

Microwells are generally small concave spaces made of a non-adhesive substrate that allow seeded cells to aggregate and form a spheroid within each well.[14,15] Commercial *AggreWell* microwell plates[16] can also be bought for direct usage but they are typically created by casting the substrate to a master mold made through 3D printing or SU-8 lithography. Common substrates used for microwells include polyacrylamide (PAAm) gel[12], polydimethylsiloxane (PDMS) polymer[17–19], and agarose gel.[11] PAAm gel is particularly interesting as not only it is highly

non-adhesive which promotes cell aggregation, it is also highly porous which allows for nutrient and oxygen exchange enabling long-term culturing of spheroids and direct analysis within the platform due to its transparency (Figure 3). Numerous arrays of microwells can be made for each casting and all the spheroids can be formed uniformly in size which is controlled through the size of microwells which can be tuned through the master mold. The entrapping nature of this particular microwell from Zhao *et al.* ensures that the spheroids stay within the platform once they are formed and simplify the handling process.[12]

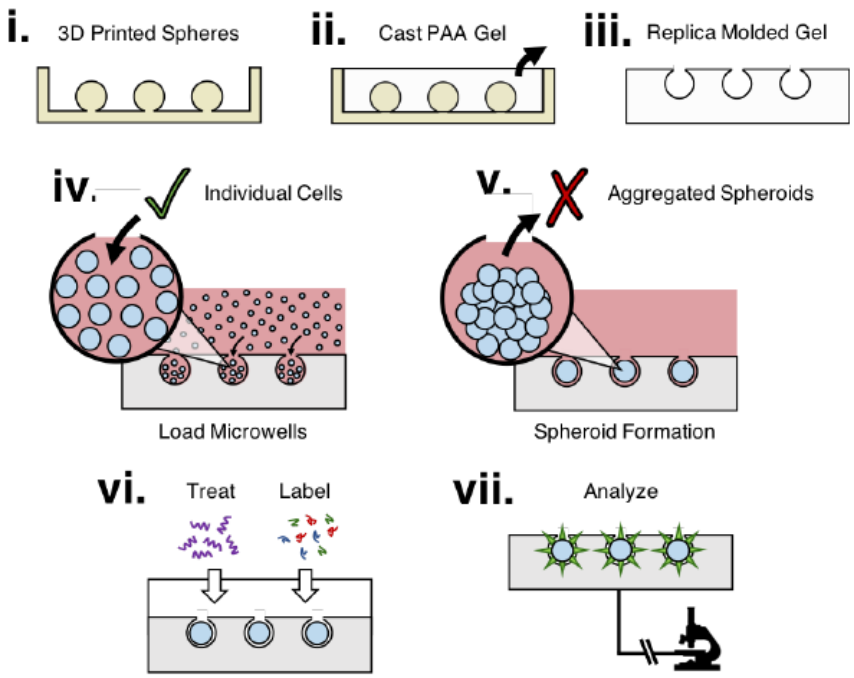

Figure 3. Spheroid formation and analysis in a PAAm microwell platform.[12]

2.1.2 Centrifugal forced aggregation

A way of using centrifugal force to form spheroids is to rotate desired cells in suspension in a low-adhesion system.[10] As the cells are constantly in movement while being unable to attach to any

substrate, they are forced to aggregate to each other to form spheroids as they have nothing else to attach to. Examples of this spheroids formation system are using rotational (Figure 4A) or spinner (Figure 4B) bioreactor.

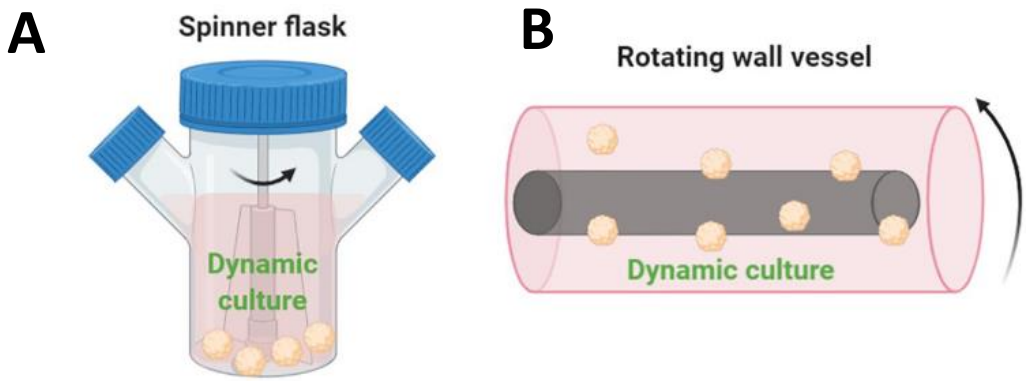

Figure 4. Centrifugal forced aggregation techniques: (A) Spinner bioreactor and (B) Rotational bioreactor from Kouroupis et al. (Frontiers).[20]

The fluid movement also improves the exchange of nutrients and waste compared to typical static spheroids. In fact, a main problem in many 3D cell culture systems is the lack of oxygen and nutrient access at the center of the culture model causing the formation of necrotic core.[21] Thus, keeping these spheroids in a moving fluid is an easier solution than vascularizing all of them. It was observed that hepatocyte spheroid could grow up to 600 µm in diameter in spinner bioreactor without formation of necrotic core.[22] Disadvantages of these techniques are that large volumes of liquid are required and more importantly the spheroids shape and size are not controlled. To improve spheroid formation consistency, cells are sometimes centrifuged downward into microwells first to promote aggregation before being transferred to a rotating bioreactor.[13,23]

2.2 Organoids

Similar to spheroids, organoids are also tissue-engineered 3D cell culture models but made from pluripotent stem cells (PSCs), adult stem cells (ASCs), or even directly sourced from biopsy samples. Unlike spheroids which generally consists of the same cells, cells forming organoids can differentiate and specialized into different type of cells and tissues. Organoids have self-organizing ability and can grow into a miniaturized 3D organs *in vitro* that can recapitulate key functionalities of *in vivo* human organs.[24,25] While spheroids are very promising as 3D culture model, organoids offer us an even more advanced tool to advance basic researches as it reduces the gap between lab cultures and animal models even closer. Today, organoids can be created for an increasing amount of organs such as gut, stomach, kidney, liver, heart, pancreas, mammary glands, prostate, lung, thyroid, retina, brain, etc.[2]

In conventional organoid culture, organoids are grown by providing the stem cells the right biochemical and biophysical cues to activate the desired morphogenetic signaling pathways at the right time to induce differentiation. Differentiated cells will segregate themselves from other types of specialized cells and it is this segregation that guides the crucial self-organization process allowing the formation of an organoid.[26] However, there are many limitations from the conventional growth methods and thus researchers have engineered novel ways of generating organoids in attempt to overcome them. I will review in more detail the limitations and the current state-of-the-art organoids engineering relevant to the platform presented in this thesis.

2.2.1 Limitations

Although organoids have been proven to be a powerful tool, many limitations arise from its complexity. One of the direct consequences of the complex protocols for organoids fabrication

is its variability. As previously mentioned, organoids formation is heavily dependent on its self-organization and differentiation cues determining cell fate decisions which are both stochastic to some degree. It has been shown through single-cell transcriptomics that organoids could have significant variations from both batch-to-batch[27,28] and organoid-to-organoid[29] depending on the type of organoid. Organoid variability is affected by their initial growth conditions (including starting cell population, positioning and aggregation), handling, and their growth microenvironment. The easiest aspect to improve would be handling and it was shown that simplifying the manual procedure for the generation of brain organoids indeed significantly decreased variability.[30] The ultimate goal would be to automate all the manual handling steps but currently the complexity of fabrication protocols still makes automatization very difficult.[2]

Another critical limitation of organoids is their restricted accessibility. Unlike *in vivo* organs, organoids are not vascularized and rely on diffusion for nutrients and waste exchanges.[31] As their size increases, cells in the middle die due to lack access to oxygen and nutrients. This causes the formation of a necrotic core, and the organoids then need to be fragmented and reformed. Additionally, many epithelial organs contain an accessible hollow core (lumen) such as heart, lung, gut, kidney, etc., but the formation of these lumen in their respective organoids is very inconsistent. Generally, these organoids are formed into an uneven spherical-shaped solid core aggregation of cells. Even when some of them successfully self-organized with lumen formation, the lumen is enclosed within the organoid and thus inaccessible (Figure 5). It then simply becomes an empty space for dead cells accumulation. This inaccessibility is a crucial limitation for these lumen containing organoids as it is often required to control both the inner and outer side of these organoids to fully study the properties of their membrane. For instance,

in studies on host-pathogen interactions or drugs absorption using intestinal organoids, both pathogens and drugs need to be delivered directly to the lumen of the organoid to simulate the right response comparable to an actual intestine.

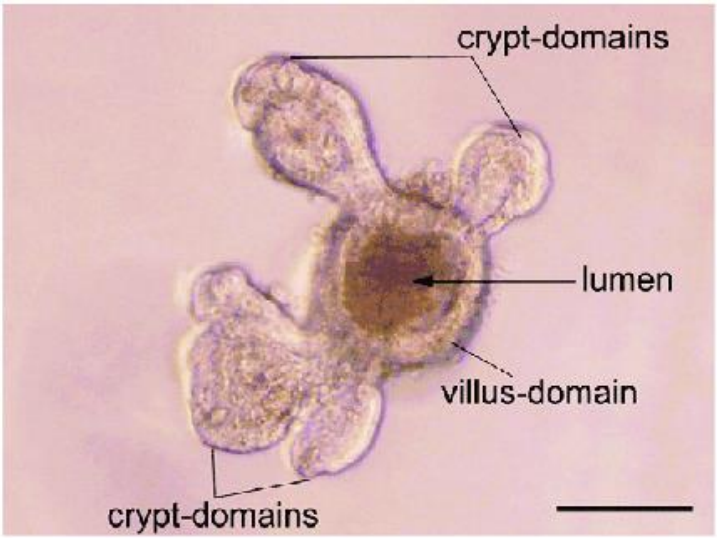

Figure 5. Intestinal organoid with enclosed lumen.[32]

Difficulty of access to different part of organoids combined with their heterogeneity of formation also brings different kinds of limitation on the ability to measured desired properties from the organoids. For example, measuring the trans-epithelial electric resistance across an intestinal organoid is nearly impossible due the challenge of probing the interior of the organoid.[33] Similarly, sampling soluble from the lumen would also either be difficult to precisely position within the organoid or simply destructive. For brain organoids, consistent measurement of electrical activity using micro-electrode array would also be highly challenging due to the variability in brain organoids causing different forming position of their lobes.[28]

2.2.2 Current organoids engineering strategies

The above-mentioned challenges pushed researchers to re-evaluate the fabrication process of organoids and develop new engineering approaches. Two general approaches at different scales have been used to redesign organoids; First is controlling the organoid by changing the inside of the cell through genetic engineering.[34,35] However, this approach is still immature as it requires a vast knowledge of cells regulatory pathways regulating differentiation which is often limited. Moreover, even though some targeted genetic modifications have shown great potential in eventually obtaining the desired organoids[36], genetically modified organoids are inherently less biologically relevant than natural organoids as the genetic modification could potentially alter organoids responses and results in studies.

The second approach to control the organoid growth is by changing the outside of the cells through engineering their microenvironment. One way is to closely control the extra cellular matrix (ECM) in which the cells are growing as it has been shown that cells interaction with ECM and other neighboring cells directly affect cell fate differentiation and is one of the key deciding factors for a successful organoid generation.[37] The controlled factors of ECM are not just chemical such as its released signaling factors[38], but also physical including its stiffness, viscoelasticity and degradability.[39] Based on this approach, researchers recently developed the next generation organoids by predefining the physical boundaries of ECM and shape-guided the organoids morphogenesis. Not only previously described spheroids generation methods such as microwells were now used for new organoids culture[40], strongly shape-controlled platforms were also developed. For instance, for intestinal organoids, collagen can be pre-formed by stamping a PDMS mold the top of collagen into villi-shape structure (Figure 6). Gut-derived cells can then be seeded on top and not only they will take the shape of the villi and crypts, but they will also

differentiate into different type of cells accordingly to their region to form a realistic intestinal organoid.[41]

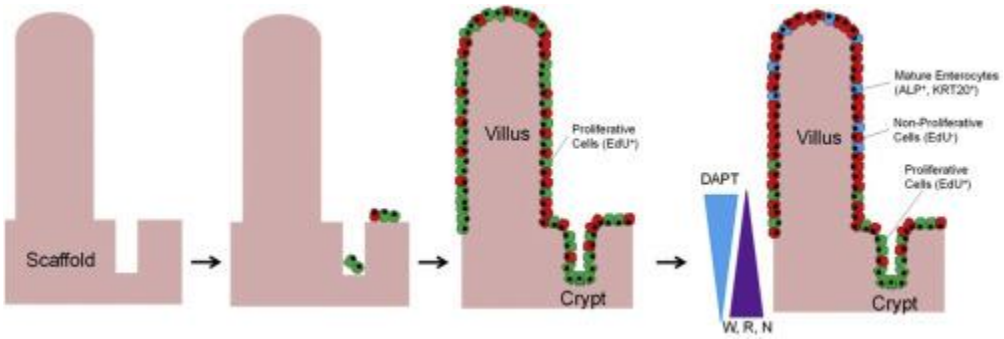

Figure 6. Microengineered collagen scaffold for shape-guided intestinal organoid morphogenesis.[41]

Other advance approaches include custom well plate with microengineered perfusable scaffolds that are embedded within cell culture developed by Lai *et al* shown in Figure 7.[42]

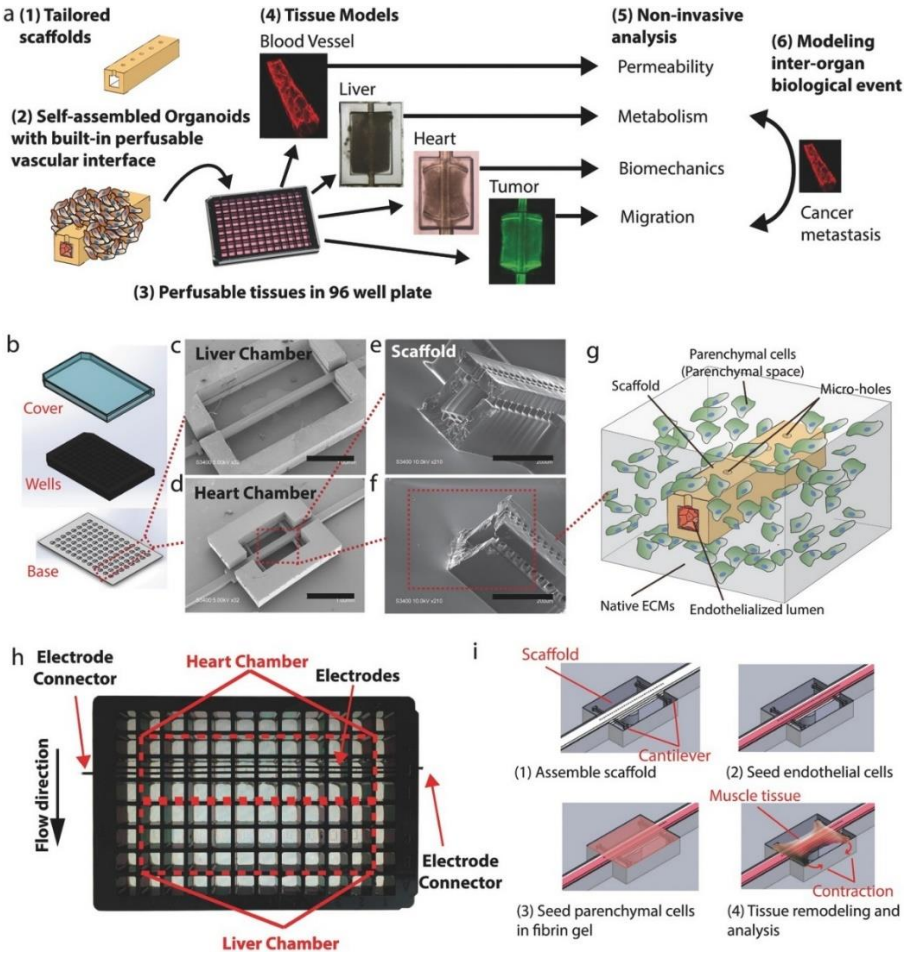

Figure 7. InVADE platform with interconnected microengineered scaffolds within each chamber that can replicate dynamic inter-organ behaviors.[42]

Not only does this platform allows the perfusion within 3D cell culture, but it also enables co-culturing to better mimic *in vivo* organs dynamic which is crucial in studies such as drug efficacy.

As 3D cell cultures requirements increase, some developed platform can precisely control the shape of perfusable vascular tissue or even the cell culture itself. For instance, *AngioPlate* from Rajasekar *et al.* shows that through predefining the shape of a dissolvable mold, a hydrogel matrix with the desired shape could be obtained and used to shape both the vascularizing tissue and organoids.[43] Another platform developed by Nikolaev *et al*. uses an advanced laser-

patterning system to outline the exact shape within a collagen matrix and then seed cells within the predefined space to form an organoid with highly controlled shape. For example, the inside of collagen can be laser ablated into villus-like structure and then let an intestinal organoid grow inside to take the shape of the lasered collagen. In this method, not only the cells differentiate and form realistic villi and crypts, but the formed lumen is also accessible as shown in Figure 8.[44] This creates a highly realistic *in vitro* intestine model useful for many studies that were previously impossible such as host-pathogen interactions, drugs and soluble absorption, etc. due to the controlled access to the inner lumen which simultaneously solves the formation of necrotic core.

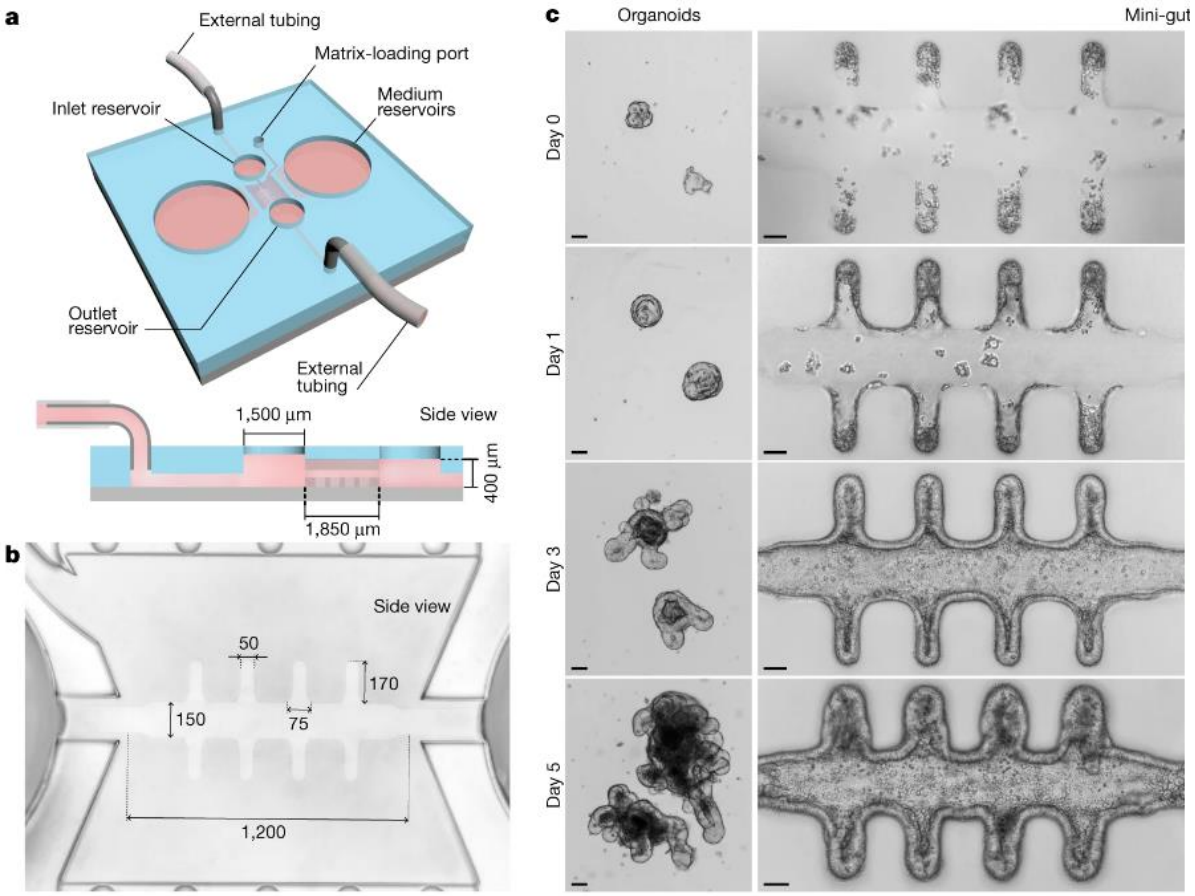

Figure 8. Laser-ablated collagen scaffold to form highly realistic intestinal organoid. Middle column shows traditionally-grown intestinal organoids in comparison.[44]

Although these platforms can create promising next generation organoids and other 3D cell culture models, it requires various intricate fabrication technologies and processes such as multilayers SU-8 lithography, and advance nano- or femtosecond laser system which are not regularly accessible for most labs.

3. Design Overview

As previously mentioned, while the conventional 3D cell cultures can recapitulate some physiological features, a critical limitation is that their uncontrolled shape cannot reproduce the physiological properties of many lumen-containing human organs such as lung, intestine, placenta, etc. where transport properties across cell layers are crucial. Even though the current state-of-the-art organoid platform could resolve these limitations, it has a very complex fabrication process requiring many tools that are not readily available for most labs.

In this work, we resolve these difficulties by engineering a glass-hydrogel microtube that can manipulate transport properties at a specific location within a 3D cell culture. Combined with microwells and centrifugal forced aggregation techniques, we can let the desired cells aggregate and form a 3D tissue over these hollow glass-sheathed hydrogel “strings” which artificially created a perfusable and lumenized “tissue-on-a-string”, enabling the delivery and sampling of desired compounds to a specific location within their core (fabrication detail described in Figure 9). This approach can hence be used to assess drug or nutrient transport within living and physiologically relevant 3D cell culture models.

1. **Insert the glass tube with the hydrogel tube through the microwell**

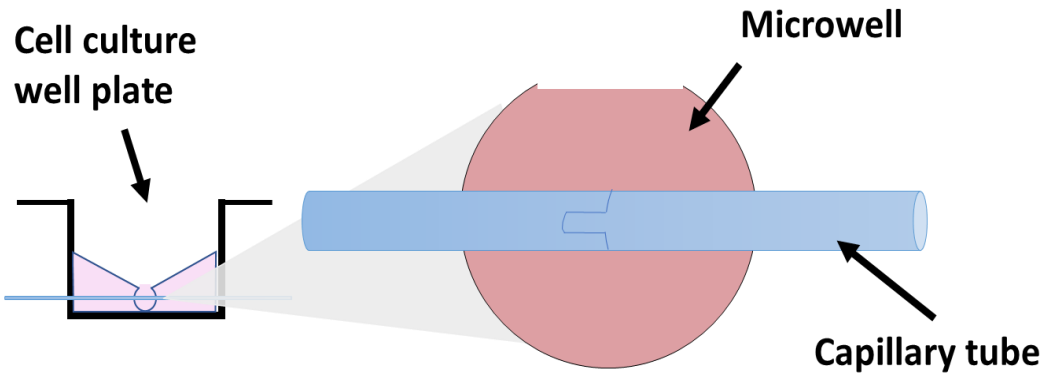

2. **Seed cells and expose hydrogel string**

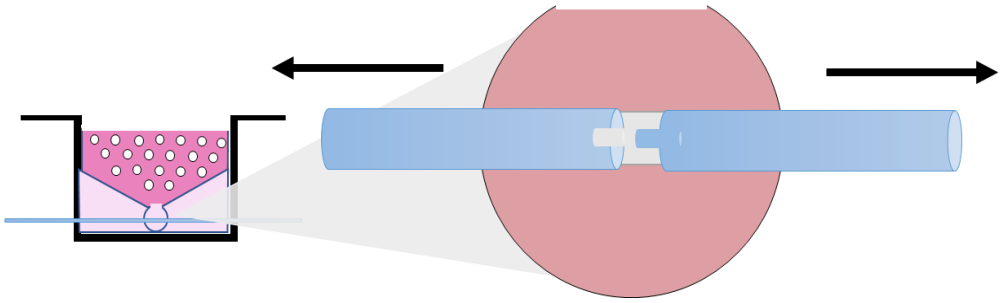

3. **Centrifuge cells down**

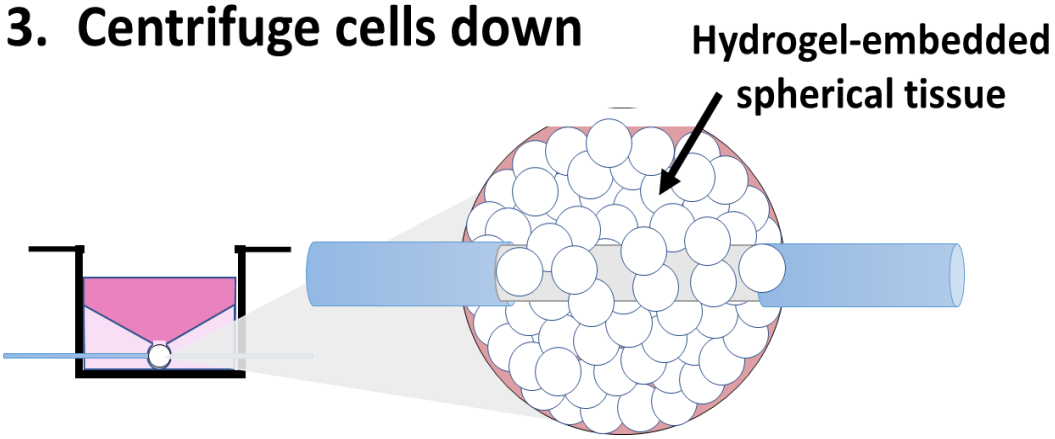

Figure 9. Tissue-on-a-string platform formation process.

4. Methodology

This section details the procedures and characterization methods used for fabrication and analysis of the proposed “tissue-on-a-string” platform. Unless otherwise stated, all cell culture materials and supplies were purchased from Fisher Scientific (Ottawa, ON), and chemicals from Sigma Aldrich (Oakville, ON).

4.1 Master mold 3D-printing

Master mold shaping the main polyacrylamide (PAAm) gel platform were designed in Fusion360 and 3D-printed using PR-57K black resin (Colorado Photopolymer Solutions) with Autodesk Ember STL 3D printer. The part was sliced at a layer thickness of 50 µm and exposure time of 1.8 s. The printed parts were washed with isopropyl alcohol placed in an ultrasonic bath and then cured under a 36 W UV light for 24 h.

4.2 Polyacrylamide hydrogel well preparation

3D-printed master mold was submerged in phosphate buffered saline (PBS) containing 1% of Antibiotic-Antimycotic (Anti-Anti) for 5 min and then air-dried prior to PAAm molding to reduce the risk of bacterial contamination. A 1 mm diameter capillary tube (Drummond) was inserted into the mold as shown in Figure 10 to form the channel in PAAm gel in which the glass-sheathed hydrogel will later be inserted.

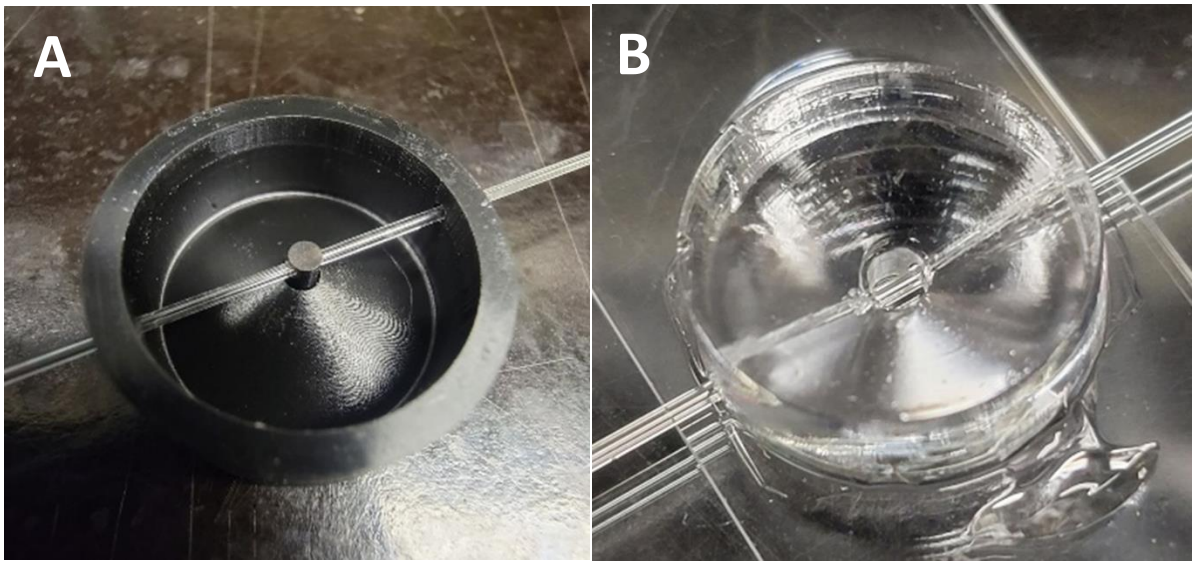

Figure 10. (A) 3D-printed master mold with capillary tube ready for PAAm gel solution loading. (B) PAAm well molded and peeled-off from the master mold.

PAAm gel was formed by mixing a prepolymer solution with an initiator prior to molding. For 1 mL of PAAm gel solution, the prepolymer solution contains 300 µL of 40% Acrylamide stock solution (Bio-Rad), 120 µL of 2% Bisacrylamide stock solution (Bio-Rad), 478 µL of PBS and 1.5 µL of Tetramethylethylenediamine, and the initiator contains 100 µL of freshly-prepared 1% w/v ammonium persulfate.[45] A 22 mm square coverslip was silanized with 0.4% 3-(trimethoxysilyl)propyl methacrylate in acetone for 5 min, followed by a 5 min rinse in just acetone and then finally air-dried. The mixed unpolymerized solution was pipetted to completely fill the 3D printed molds and silanized cover slips were placed on top of the mold to block the solution from air and binds to PAAm gel during polymerization.[46] After 6 min of gelling, the capillary tube was first removed from the gel-containing mold by slowly sliding it out from one side through the gel and then the coverslip was peeled off from the mold with the gelled PAAm well attached. It was then rinsed and stored in PBS for at least 24 h to remove residual acrylamide and to allow the gel to finish swelling.

4.3 Fabrication of glass-sheathed hydrogel microtube

Two 24-gauge dispensing tip were inserted on each side of a 7.5 cm long capillary tube with an outer and inner diameter of 1 and 0.78 mm respectively. The thicker capillary tube provides a tighter seal once inserted into the PAAm well with preformed channel. A nickel-titanium (NiTi) wire of 254 µm diameter was wiped with 70% ethanol and threaded into the capillary tube through both needles. 1% agarose gel was heated up for 20 seconds in a microwave and then quickly injected in the capillary tube with a syringe. As the agarose cooled down and gelled within a minute, the metal wire was pulled in tension while the needles centered the wire within the capillary tube allowing a straight agarose channel to be formed. Metal wire was finally slowly pulled out from one side and the needles were removed (Figure 11).

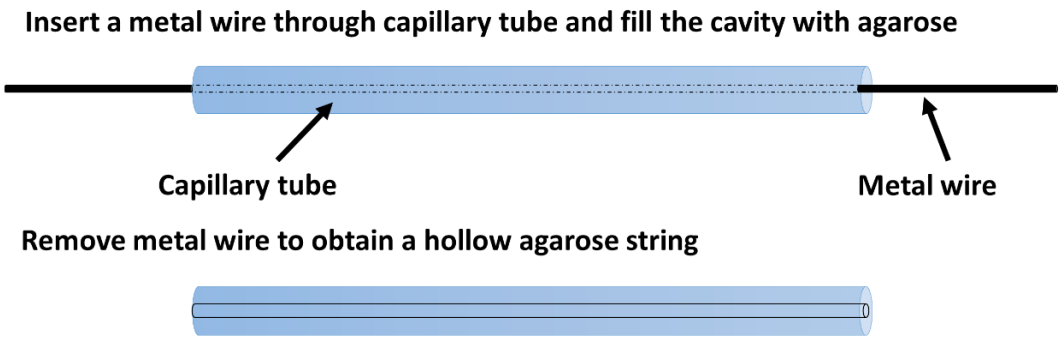

Figure 11. Glass-sheathed agarose tube fabrication.

4.4 Preparation of tissue-on-a-string device

A small hole was punctured on each side of a 35 mm cell culture dish with the tip of a soldering iron and the PAAm well was placed inside the dish with the channel aligned with the holes. A slight cut was made at the middle of the agarose-containing capillary tube with a cutting tile and then carefully inserted through the dish and the preformed channel in the PAAm well. Once the

cut was centered with the well opening, the capillary tube was carefully broken exposing a ring of agarose gel inside the PAAm well. The needles were re-inserted into each side of the capillary tube and the open junctions as well as the openings on the sides of cell culture dish were sealed with Loctite 3525 (Diverse Electronics), an UV curable adhesive. Loctite must be completely cross-linked under UV to avoid the release of toxic material in contact with aqueous solutions.[47] More PAAm prepolymer solution was mixed and added in the dish around the centered PAAm well to secure its position and to seal potential leaks from the pre-formed PAAm channel. PBS with 1% Anti-Anti was then both flowed through agarose string at 50 µL h^{-1} with a syringe pump and also used to submerge the PAAm gel for at least 24 hours prior to cell culture to rinse off residues and avoid bacterial infection.

4.5 Cell culture

Both T-47D breast cancer cells (ATCC; HTB-133) and BeWo human placental choriocarcinoma cells (ATCC; CCL-98) were cultured in 10% fetal bovine serum (FBS) and 1% Anti-Anti in Dulbecco Modified Eagle Media (DMEM) in an incubator at 37^{o}C and 5% CO_2. Culture media was changed every two days. When cells reached confluency, trypsin-EDTA (0.25%) was used for 5 min to dissociate cells from the cell culture flask and resuspended in culture medium at a subcultivation ratio of 1:3. Cells were discarded once reaching the 24th passage.

4.6 Device seeding and tissue-on-a-string formation

Prior to cell seeding, PBS in the PAAm well was aspirated exposing the capillary tube. It was then coated with type I bovine collagen (Advanced Biomatrix, 3 mg mL^{-1}) diluted to 0.1 mg mL^{-1} in PBS for 24 h at 37^{o}C which allowed cells to attach to the glass surface of the capillary tube and forming

a seal around the exposed agarose string.

A confluent T-25 cell culture flask containing around 2.5×10^6 cells was suspended in 200 µL of medium and pipetted into the PAAm well. The device was then lightly centrifuged at 25 G for 5 min to help settling the cells inside the well. The cells were guided into the well through the funnel shaped opening. The device was finally left in the incubator for 24 h to allow the cells to attach to each other and to the capillary tube forming a 3D tissue culture around a hydrogel string.

4.7 Formation of fused BeWo-on-a-string

After BeWo spheroid was formed according to the method described in section **Error! Reference source not found.**, 24 µM forskolin dissolved in cell culture medium was added on top of the spheroid and also flowed through the agarose string at a low flowrate of 5 µL h^{-1} for 48 h to limit flow disturbance. The forskolin containing medium on top of the spheroid was changed after 24 h. This induced *in vitro* fusion of the cells from both the center and outside of the BeWo spheroid. Higher forskolin concentration at 48 µM were also used to form BeWo spheroid with increased fusion.

4.8 Fluorescein-tagged dextran flow through the tissue-on-a-string

Fluorescein-tagged dextran were dissolved in cell culture medium at 1 mg mL^{-1}. and flowed through the agarose string at 50 µL h^{-1} with a syringe pump to deliver dextran to the center of the 3D tissue. 10 and 500k dextran were used to compare BeWo spheroid diffusivity at different forskolin concentrations.

4.9 Particle image velocimetry

Fluorescent beads of 1 µm were diluted in PBS to 5 µL mL^{-1} and flowed through the agarose tube with the syringe pump flowrates set at 50, 100 and 1000 µL h^{-1} to determine their respective flow velocity within the tube. The exposure time of the microscope was set to 1 second and the resulting images show the beads forming a line in the direction of their travel. The length of the line indicates the distance that specific bead travelled in 1 second and corresponds to the flow velocity. Since the length of the lines indicated a parabolic flow profile, the maximum center velocity was used to approximate the flowrate within agarose tube.

4.10 COMSOL modelling

A 2D axisymmetric time-dependent finite element model was built in COMSOL v.6.0.0.318 (COMSOL Inc., Burlington, MA, USA) to simulate mass transport in the glass-hydrogel microtube device. In this model, solutes carried by culture media (modelled as water) in the microtube establish a driving force for diffusion across the agarose wall into the microwell cavity. More specifically, convection in the microtube sets the solute concentration at the inner hydrogel wall and the latter determines diffusion across the rest of the device. Flow within the microtube was modelled as laminar with a no-slip boundary condition and a fully developed inlet flow rate of 50 µL h^{-1}. In addition, the solute concentration was set to 10 mM at the inlet and diffusion coefficients were varied for each simulation (Table 1). All concentration profiles were obtained when steady-state was achieved, and the total molecular flux was measured at the hydrogel-cavity interface. For all studies, a free triangular mesh was used and optimized to ensure a coefficient of variation of less than 1%.

Table 1 - Diffusion coefficients for various solutes in water and agarose hydrogels [$\mu m^2/s$] taken from Shoga et al.[48]

		Medium	
		Water or 1% agarose	5% agarose
Solute	Fluorescein	450	250
	3kDa dextran	150	100
	10kDa dextran	100	80

A full 3D model was also created to simulate diffusion within the well cavity (Figure 12). Source concentration on the outer surface of agarose was set to 10 mM and the diffusion coefficient was varied between 10^2 to 10^4 μm^2 s^{-1}.

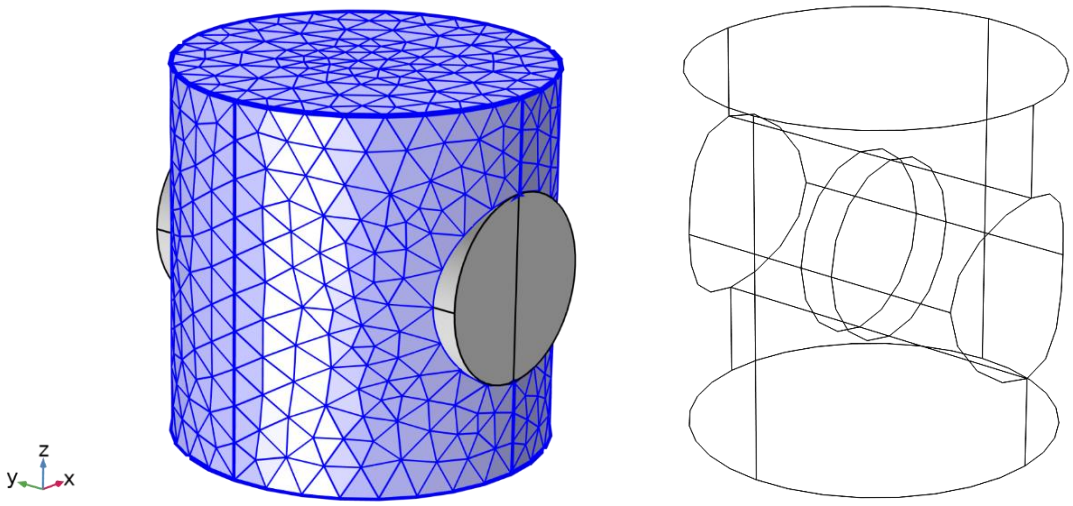

Figure 12. Mesh and geometry of the 3D finite element-based modelling of diffusion in well cavity.

To compare the simulated results to the observed fluorescence intensity, the vertical concentration values of the bottom 500 µm (on z-axis) of thickness along the x and y- centerlines were obtained and summed for each x and y coordinates to simulate the concentration intensity

profile of fluorescence as captured by the microscope. In short, a 2D projection of the fluorescence intensity from the bottom of the well as it would be observed from the microscope lenses was estimated using the modeled values for comparison.

The obtained diffusion curves were fitted as gaussian distribution using the Curve Fitter function built in the Statistic and Machine Learning Toolbox from MATLAB (MathWorks Inc., Natick, MA, US). Fitted equation was given in the following format:

$$y = a * e^{\left(-\left(\frac{x-b}{c}\right)^2\right)} \qquad \textit{Equation 1}$$

a is amplitude, *b* is the centroid and *c* describes the width of the curve which can be used to calculate variance (σ^2) through the following relation:

$$\sigma^2 = \frac{c^2}{2} \qquad \textit{Equation 2}$$

5. Results

5.1 Tissue-on-a-string platform

The final design of tissue-on-a-string platform is shown in Figure 13 below.

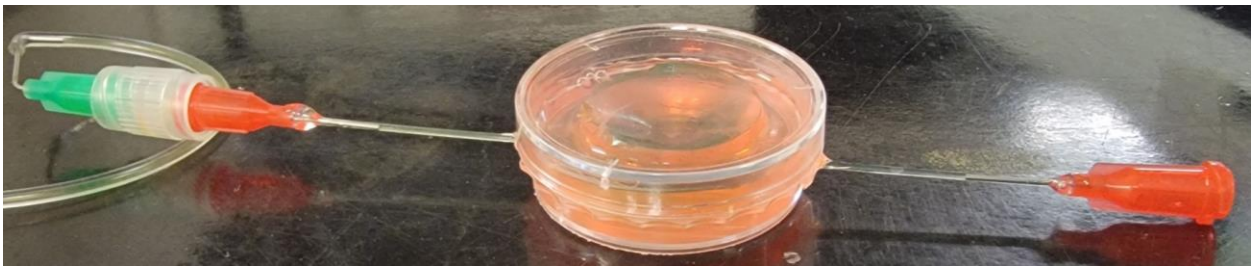

Figure 13. Tissue-on-a-string platform.

Unlike conventional hydrogel microwells, the seeding surface has been tapered into cone shape to guide all the seeded cells towards the well for 3D tissue formation through centrifugation

without any wasted cells. The agarose gel string is pre-implanted within the well and as the cells aggregate in the well and form the 3D tissue, the agarose string acts as an “artificial lumen” and can be used as the delivery and sampling medium. Although agarose gel is very porous, fluid diffusion through a thin and long agarose string still requires a large driving force. A simple experiment showed that it takes around 1 hour for fluid to diffuse through a 10 cm capillary tube filled with solid agarose gel at a syringe pump flow rate set to 500 µL h^{-1}. To increase the speed of delivery, a Nickel-titanium (NiTi) wire of 254 µm thickness is centered through the capillary tube before agarose injection and gelation. Upon removal of the wire, a hollow agarose tube is formed, and this reduces the fluid diffusion resistance to a thin wall of agarose gel of 263 µm at the delivery point instead of across the whole length of the agarose string. The entire PAAm well and the 3D tissue are enclosed within a 35 mm petri dish to maintain sterility while the capillary tube openings are exposed outside of the dish for easy tubing connections accessibility. To demonstrate that the platform is functional, T-47D, a breast cancer cell line commonly used to form 3D spheroids, were seeded into the polyacrylamide gel well and formed a viable spheroid-on-a string after 1 day (Figure 14).

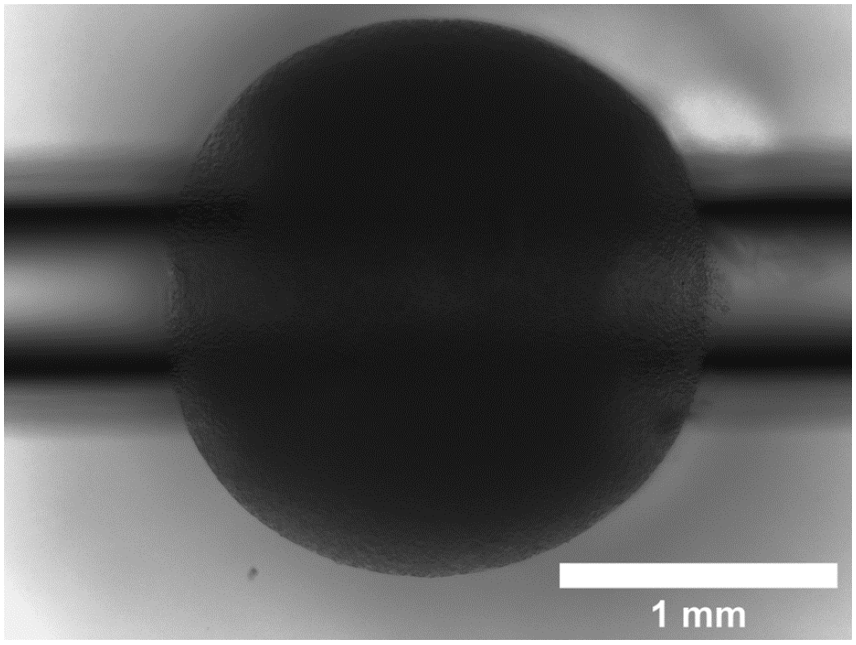

Figure 14. Spheroid-on-a-string formed with T-47D cells.

5.2 Point source delivery characterization

When connecting tubing directly to the gel-containing capillary tube, the fluid flow creates a tangential pressure on the opening of agarose gel due to reduction of channel diameter at the interconnection which damages the gel and blocks the channel. An extra thin flexible injection needle is inserted into the agarose tube opening to initiate the fluid flow within the gel. However, with the addition of such needle, the fluid flowrate is not conserved between inside the agarose tube and syringe pump since the agarose tube opening is not perfectly sealed around tip of the needle. Thus, particle image velocimetry (PIV) was used to quantify actual flowrates at different syringe pump injection speed (Figure 15).

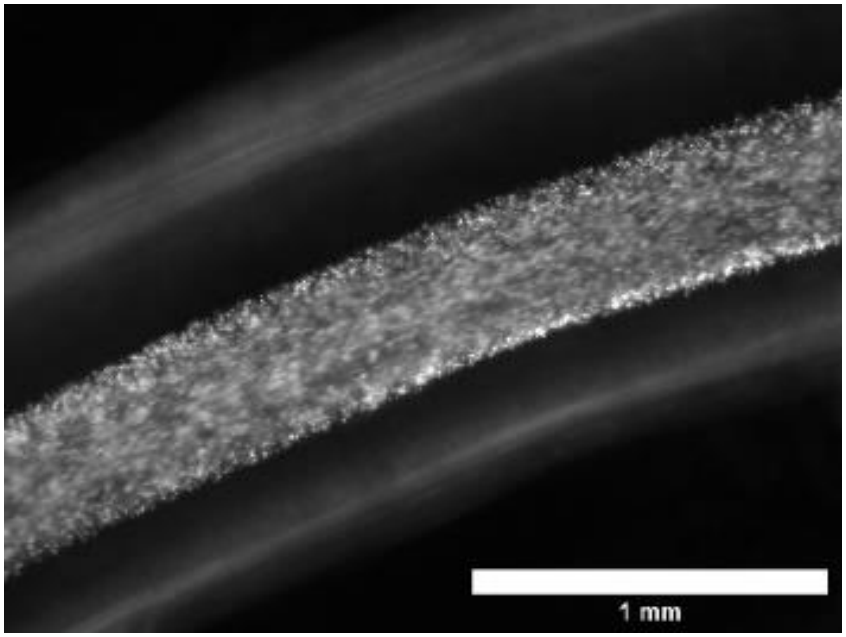

Figure 15. Flow within hydrogel microtube characterized by fluorescent beads.

Fluorescent microbeads revealed the fluid flow under microscope and a parabolic flow profile was observed inside agarose tube with an almost no-slip boundary. Centerline velocities were measured to approximate flowrates for simplicity and results are shown in Table 2

Table 2 – Flow velocities within hydrogel microtube at different syringe pump flowrates

	Direct connection	With injection needle at connection	
Syringe pump flowrate [µL h^{-1}]	**Measured max velocity [mm s^{-1}]**	**Measured max velocity [mm s^{-1}]**	**Approximate max flowrate within agarose [µL h^{-1}]**
50	N/A	0.30	54
500	N/A	1.27	231
1000	N/A	1.98	361

At a low syringe pump flowrate of 50 µL h^{-1}, the fluid flow is relatively conserved in the agarose tube (slightly higher approximate flowrate of 54 µL h^{-1} due to the use of max centerline velocity for calculation) compared to higher flowrates of 500 and 1000 µL h^{-1} where less than half of positive fluid flow is conserved caused by the resistance of such small channel and thus creating backward flow. A low syringe pump flowrate of 50 µL h^{-1} was used for other experiments as it is conserved properly in agarose tube.

Point source delivery of a model compound was demonstrated by flowing fluorescein isothiocyanate (FITC) and analyzing its brightness at the delivery point in an unseeded empty well at a flow rate of 50 µL h^{-1} (Figure 16). FITC fluorescence illuminated through agarose after only 5 minutes and stabilized at 1 hour.

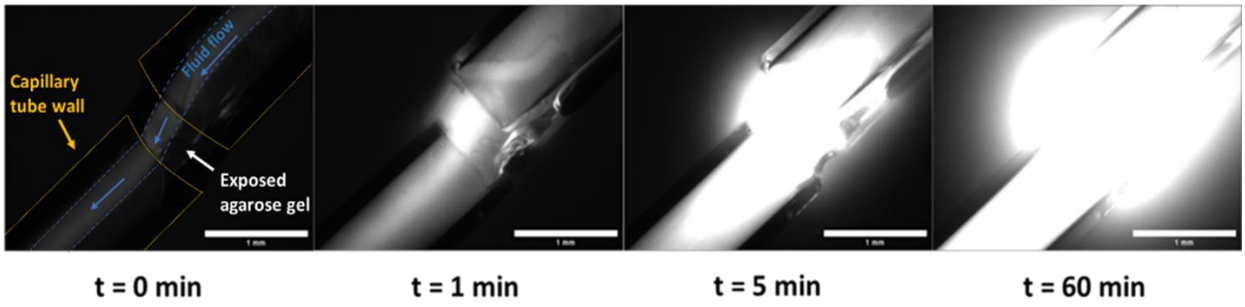

Figure 16. Characerization of point source delivery progression timeline.

5.3 Finite element-based modeling of mass transport in microtube

Finite element modeling was used to better characterize mass transport in the glass-hydrogel microtube so it could be characterized prior to analysis on cell culture. Solute diffusion through agarose at the delivery point was modeled and shown in Figure 17 below.

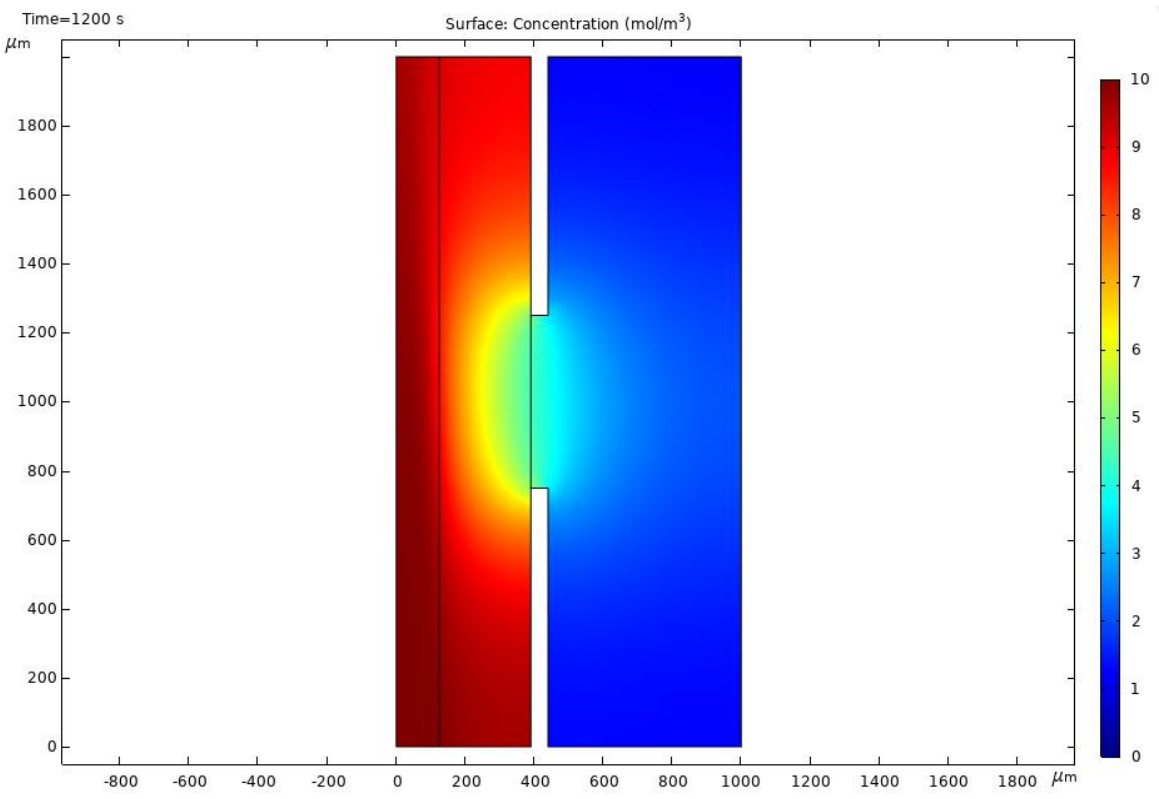

Figure 17. Spatial concentration profile at the delivery point of the glass-hydrogel microtube.

In agreement with the point source delivery characterization from previous section, diffusion limitations are minimal through the agarose wall as the fluorescein concentration at the delivery point increases instantaneously and reaches steady state after around 20 minutes at a flowrate of 50 µL h^{-1}.

The model also shows the theoretical maximum concentration at steady state to evaluate the delivery efficiency of solutes of various sizes (Figure 18).

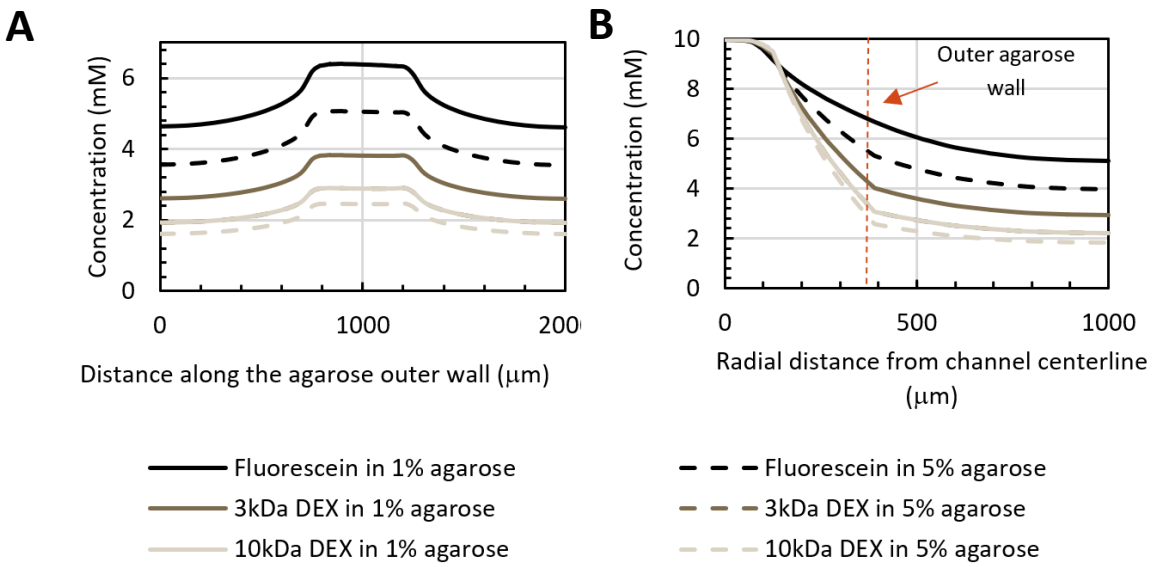

Figure 18. Modeled concentration profiles at a delivery flowrate of 50 μL h^{-1} after 1 hour. (A) Concentration along the agarose outer wall at the delivery point. (B) Concentration profile along radius from the centerline of microtube.

After 1 hour of delivery, the concentrations of smaller molecules such as fluorescein or 3kDa dextran on the outer surface of agarose at the delivery point are relatively high as more than half of the source concentration is maintained. However, for 10 kDa dextran, a larger molecule, less than 30% of the source concentration is delivered across agarose. This is also shown by the significant lower theoretical flux of larger dextran molecules (Figure 19).

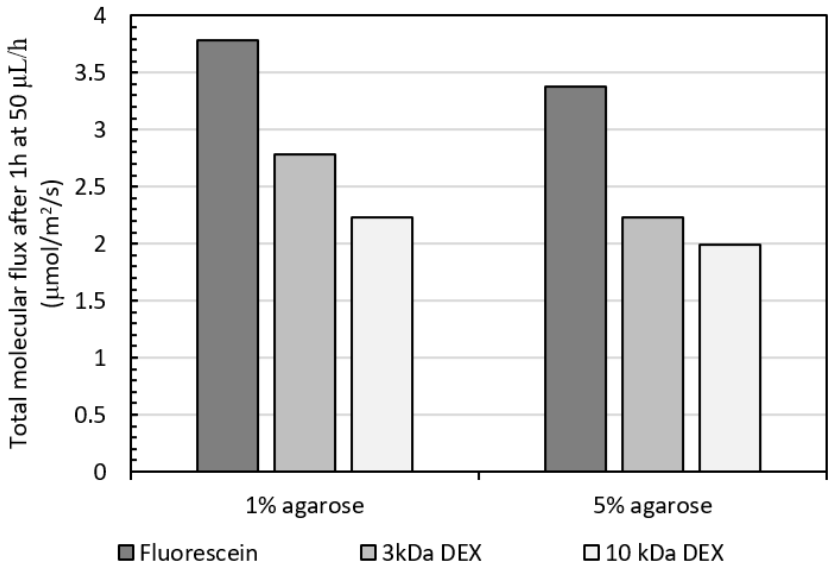

Figure 19. Total molecular fluxes of solutes at a flowrate of 50 µL h^{-1} at steady state after 1 hour of delivery.

5.4 BeWo spheroid diffusivity

Our device was used to study the transport of different sizes solute across BeWo trophoblast, a human placental cell line commonly used as *in vitro* placenta model, and the effect of forskolin concentration on its diffusivity. Fluorescein-tagged dextran was point source delivered to the core of forskolin-treated BeWo spheroid for 1 h at 50 µL h^{-1} under 3 different conditions shown in **Error! Reference source not found.**. Briefly, dextran of 2 different molecular mass (10 and 500 kDa) and 2 different forskolin concentrations treatment (24 and 48 µM) were tested and compared against each other.

Table 3 – Dextran size and forskolin concentration for each condition

	Condition		
	1	2	3

Dextran size [kDa]	500	10	10
Forskolin concentration [µM]	24	24	48

Media containing dextran that is on top of the spheroid in the well was collected after each experiment and its dextran concentration was measured through its fluorescence with a calibration curve (Figure 25) and the results are shown in Figure 20.

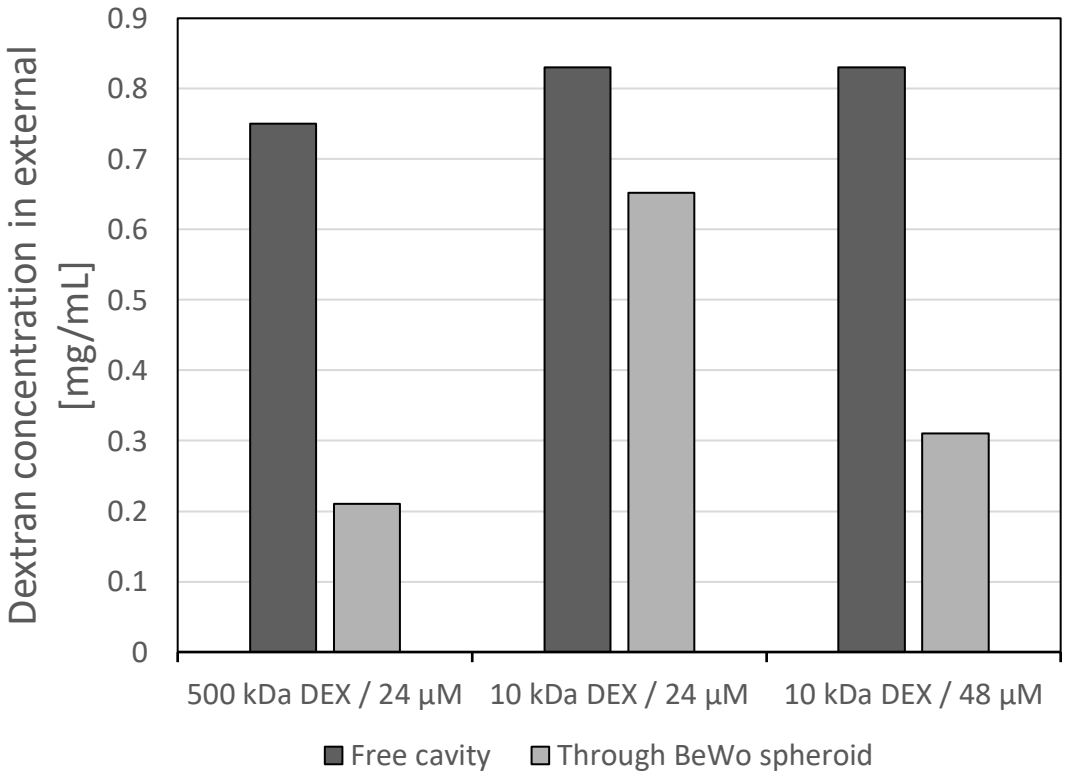

Figure 20. Dextran concentration in media collected on top of the BeWo spheroids.

Since diffusion of dextran also occurs within agarose, deliveries for 500 and 10 kDa dextran were first performed within empty well for 1 hour and then the media within well cavity were collected as base concentration values to compare the relative concentration decreases in the presence of

BeWo spheroid when the dextran molecular sizes were different. As expected, at the same forskolin concentration of 24 µM, a higher decrease in concentration of -72% were measured for 500 kDa dextran as compared to -21% for 10 kDa due to its larger molecular. On the other hand, with the same dextran size of 10 kDa, a lower dextran concentration of 0.31 mg mL^{-1} was collected on top of the BeWo spheroid treated with higher forskolin concentration as compared to 0.65 mg mL^{-1} of the BeWo spheroid treated with lower forskolin concentration. Assuming a linear relationship between concentration difference and diffusion coefficient based on Fick's law, doubling the forskolin concentration on BeWo spheroid roughly halved the diffusion coefficient of 10 kDa dextran. Since the main goal was to measure correlation and trend between molecular size and forskolin concentration to diffusion, only one sample was used for each condition.

For each experiment, fluorescein-tagged dextran can clearly be seen under microscope to diffuse through the BeWo spheroid from its center (Figure 21).

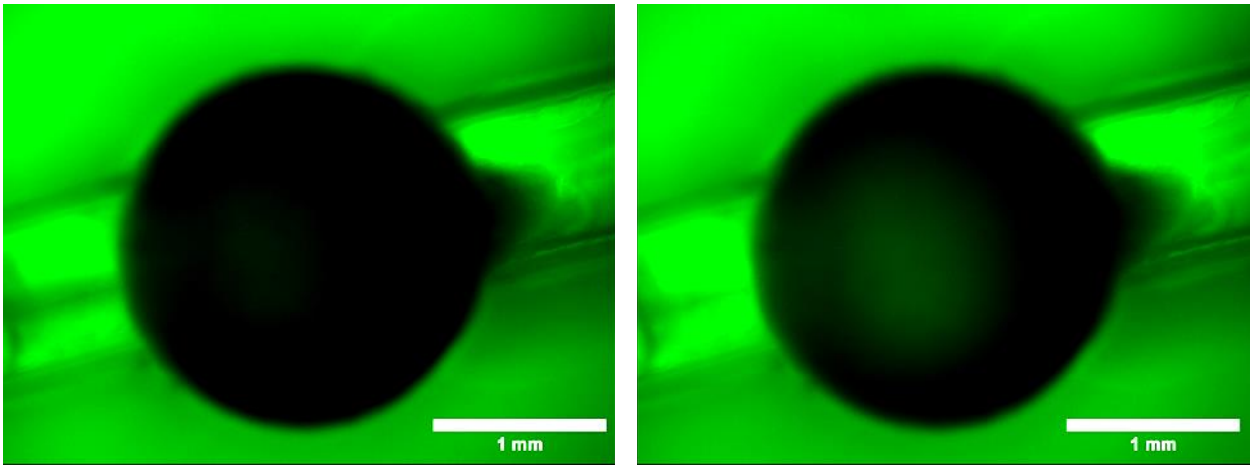

Figure 21. Comparison of dextran intensity under fluorescence microscope before and after dextran delivery for 1 hour.

The concentrations of dextran were estimated by its fluorescence intensity. However, the absolute concentration of dextran inside the spheroid could not be obtained accurately as its fluorescence is obstructed by BeWo cells. Thus, the fluorescence intensities inside the spheroid were obtained only to plot the relative concentration profile of dextran throughout the delivery (Figure 22).

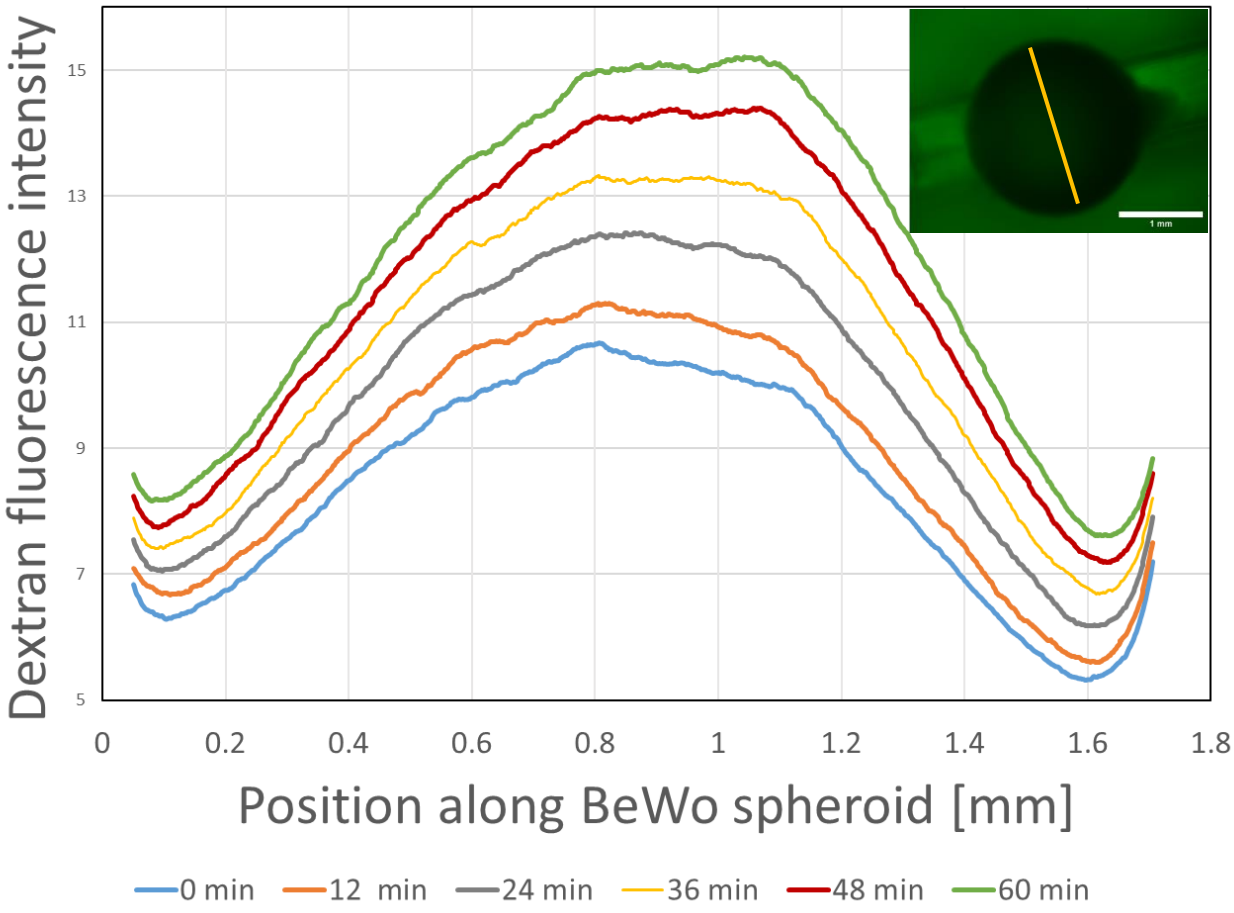

Figure 22. Relative concentration profile of 500 kDa assessed perpendicularly across the BeWo spheroid throughout 1h of point source delivery.

To better analyze the fluorescence intensity distribution profile observed from microscope, simulated intensity profiles were obtained from a finite element modelling of the full diffusion inside the 3D well cavity (Figure 23).

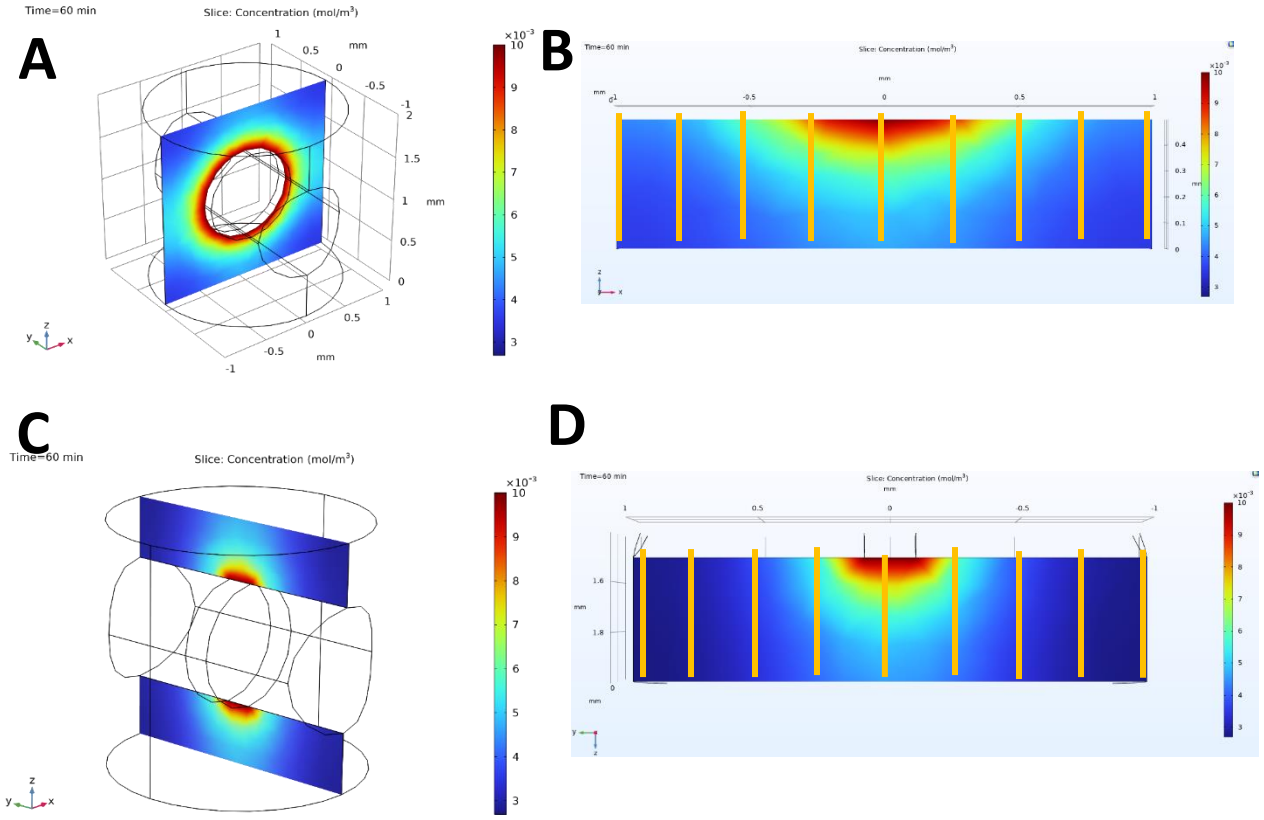

Figure 23. Concentration profiles from COMSOL modeling of diffusion within well cavity after 1 hour. (A) Streamlines. (B) Perpendicular slice at the delivery point. (C) Bottom 500 µm of the perpendicular slice that could be observed by microscope. (D) Parallel slice at the delivery point. (E) Bottom 500 µm of the parallel slice that could be observed by microscope.

Since the microscope observes the well cavity from the bottom and the dextran fluorescence would be stacked up to produce the final observed intensity, the simulated intensity profile that would have been obtained under the microscope was obtained by summing up the concentration values along the drawn yellow lines in Figure 23B and D along the centerline for both parallel and perpendicular to the microtube.

We found through modelling that the shape of the gaussian distribution does not vary with diffusion coefficient or initial source concentration value and that only the absolute intensity value was changing along the curve. Thus, both simulated intensity curve and the observed curve at 60 minutes of delivery were normalized to compare the shape of their curve (Figure 24).

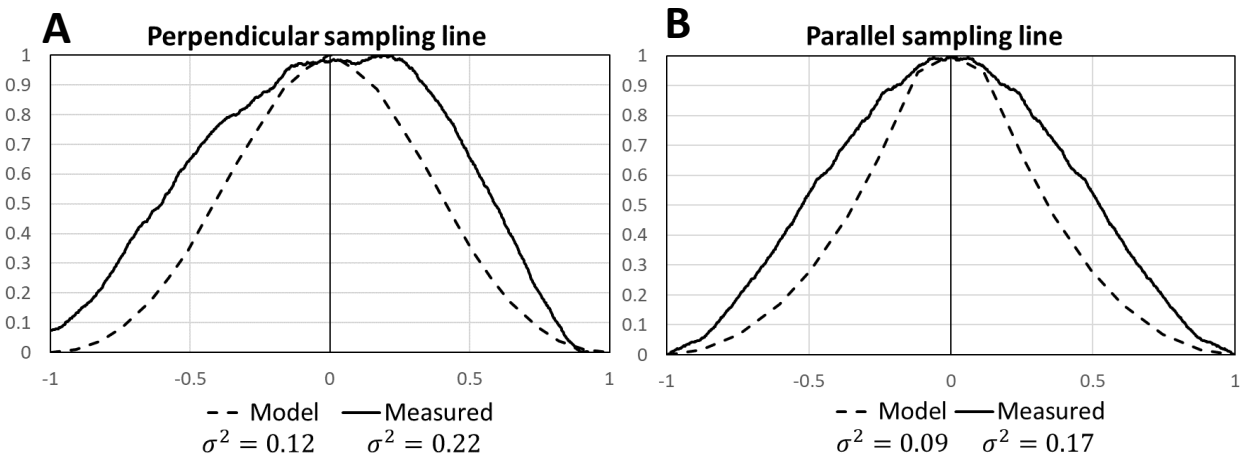

Figure 24. Modeled and measured fluorescence intensity curve observed from microscope after 1 hour. (A) Along perpendicular and (B) parallel sampling line; Model curve obtained from perpendicular and parallel slice at delivery point respectively.

For both perpendicular and parallel sampling line, the variances of the measured curves are significantly larger than the modelled values (by approximately 85% for both curves).

6. Discussion

6.1 Materials and design considerations

Tissue-on-a-string platform is highly inspired from the work of Zhao *et al.* on polyacrylamide microwells.[12] Polyacrylamide is a well-established biocompatible hydrogel permitting oxygen and nutrients transfer.[49,50] It has previously been demonstrated to be a viable material to form 3D cell culture when shaped as micropockets due to its low cell attachment property.[8] On the other

hand, agarose, a biocompatible polysaccharide polymer, is chosen as the string material due to its excellent physiochemical properties supporting cell growth and drug delivery.[51] Agarose gel in general has a larger pore size compared to polyacrylamide gel as the latter is often used to separate shorter nucleic acids during gel electrophoresis (requiring smaller pores) as opposed to large DNA fragments for the former.[52] This property is particularly useful in maximizing diffusion in this platform. The hydrophobic properties of agarose gel[53] also minimizes gel tearing during the fabrication of the hydrogel tube as it is less likely to bind to the capillary tube compared to polyacrylamide gel which is hydrophilic.[54]

The formed 3D culture is 2 mm in diameter which is relatively large compared to traditional spheroids that are usually around 400 to 700 μm.[55] This is due to the need of the tissue to be slightly larger than the capillary tube used (1 mm outer diameter in this case) to encapsulate the delivery point. The culture size could be reduced with the use of smaller capillary tubes and thinner wires to reduce its interference with the tissue, although it would increase the fabrication difficulty. On the other hand, the platform could easily be scaled up to form even larger size 3D cell cultures without necrotic core formation[21] due to the embedded artificial lumen.

To increase the point-source delivery speed of the platform, NiTi wire was used to create a hollow agarose tube. NiTi wire has been chosen as it has been shown to be compatible with various biomedical applications such as implantation.[56–59] In addition, its outstanding elasticity coupled with shape memory properties[60] allowed the wire to be pulled into a perfect straight line consistently without any difficulties on top of being reusable. While wires of other materials

could also achieve the same results, NiTi wire greatly simplified the fabrication process.

The point source delivery rate can be controlled through syringe pump flowrate but also the area of exposure of agarose gel. However, since the latter is difficult to control, fluid delivery rate was only controlled through syringe pump flowrate while keeping the exposing area consistent by only breaking the capillary tube without actively pulling it apart to expose agarose gel extensively. However, the dextran diffusion experiments still showed inconsistencies with finite element modeling in which it was estimated that only 30% of the source concentration could be delivered across agarose gel to the well cavity for molecules larger than 10 kDa while approximately 90% of the source concentration was retained during the benchmark deliveries of 500 and 10 kDa dextran as shown in Figure 20. We reason that this discrepancy might be due to some dextran containing media flowing in between the capillary tube wall and agarose gel as some back flow is created at the entrance and then forced through the slit. Even though this delivery method is different from the intended way, it essentially allows a more direct delivery within the core of the 3D cell culture without significant loss in soluble concentration.

6.2 Diffusion within BeWo spheroid

BeWo trophoblast is a human placental cell line commonly used as *in vitro* placenta model for the studies of nutrients uptake.[61] After 2 days of forskolin treatment, BeWo trophoblast cells can fuse to become syncytiotrophoblast which is a multinucleated cell layer that regulates transport between the mother and fetus[62] and thus is a well-established cell line used for fundamental studies of fusion.[63,64] However, the formation of large BeWo spheroids has been difficult compared to other cell lines that are commonly used in 3D cell culture such as T-47D. BeWo cells

showed a lot of attachment issues as the top part of the spheroid were often lost during forskolin treatment and handling. Thus, extra care in handling was given to BeWo spheroid formation but still resulted in lack of repeated experiments. The 3 experiments conditions were set up to compare the effect of molecular mass and forskolin concentration on the diffusivity within BeWo spheroid. For both 500 and 10 kDa, the concentrations of dextran delivered into an empty well were relatively similar (0.75 vs 0.83 mg $mL^{-}1$ respectively). In the presence of BeWo spheroid, the final concentrations in the collected media were considerably lower for the larger molecules (0.21 vs 0.65 mg mL^{-1} for the smaller 10 kDa dextran). This fundamental comparison experiment shows that the BeWo spheroid is indeed nicely formed in our platform and provide enough resistance for mass transport studies within the tissue.

Studies have shown that fusion of BeWo cells can be stimulated by forskolin, an inducer of syncytialisation, to form multinucleated syncytiotrophoblasts[64,65], and thus was used to treat our BeWo-on-a-string to study its effect on soluble diffusion within the BeWo tissue. The original hypothesis of this experiment was that an increase of forskolin concentration would lead to more BeWo cells fusion and consequently decreases the tissue diffusivity. However, even though it was shown that higher forskolin concentration indeed decreases diffusion within BeWo spheroid, we couldn't confirm if it was due to higher amount of cell fusion due to the unsuccessful staining of syndecan-1 (SDC-1) which is generally used to indicate syncytia formation (shown in Appendix 8.2). To further investigate the reason behind the decrease of diffusivity, a side experiment consisting of adding forskolin of various concentrations to regular BeWo membranes grown on PAAm gel. It was observed that higher forskolin concentrations induces a contractile behavior in the cellular membrane (Appendix 8.3). At forskolin concentration higher than 75 µM, BeWo

membrane starts to detach from the well plate and pulls itself tighter together forming a small aggregate of cells. Therefore, we reason that the observed decrease in diffusivity could result from this contractile aggregation behavior of BeWo cells at higher forskolin concentration.

Although only a 2D projection of the relative concentration profile within BeWo spheroid could be obtained through fluorescence microscope, finite element modeling allowed us to compare the measured profile to a theoretical one. Both measured and modeled curve exhibit a gaussian distribution commonly shown in many diffusion processes. However, since the finite element modeling showed that the shape of this gaussian distribution does not change with the magnitude of diffusion coefficient of initial source concentration, the wider curve from the measured profile shown by the higher variance could be indicating a non-homogeneous diffusion coefficient within the spheroid. The significant higher variance in the measured curve indicates there is higher diffusion closer to the source compared to the model with uniform diffusion coefficient. The diffusion coefficient is thus higher at the center of the spheroid and gradually decreases towards the edge. This could be due to the spheroid compaction which is driven by a contractile outer shell as shown in Lee *et al.* resulting in a higher cell density in outer layers and consequently decreases diffusion in that area.[66] This was also observed on the BeWo membranes treated with 75 and 100 µM forskolin shown in Appendix 8.3 which exhibit a thicker outer ring on the edge of the membrane patch.

To assess whether the simulated imaging depth affects the variance of the obtained curve, the modeled fluorescence intensity curve for a lower imaging depth of 300 and 100 µm was also obtained. It was found that the variance increases from 0.12 (for the original assumed imaging

depth of 500 μm) to 0.13 and 0.134 respectively for perpendicular sampling line (shown in Appendix 8.4). This shows that the variance of model gaussian distribution curve is slightly dependent on the summing depth of the concentration profile. Even though there is a positive correlation between the simulated imaging depth and the variance of distribution curve, the increase is so minimal that we concluded the significantly larger variance from the measured distribution curve was still result of uneven diffusion within BeWo spheroid.

6.3 Future work and applications

In this thesis, we showed the potential application of the tissue-on-a-string platform through a placenta model. *In vitro* placenta cell culture models are of great importance due to ethical and safety concerns of *in vivo* studies in humans as it involves pregnancy. As demonstrated, our BeWo-on-a-string could be used as a quick diffusion assessment platform for placenta but it also has great potential to become a rapid drug screening platform as it can simultaneously determine the potential effect of the drug on placenta and its diffusivity through the tissue which could be indicative of its potential exposure to the fetus.

Not only the microtube can be used as a point source delivery tool as shown in this thesis, but it could also be used as a collecting tool. A neutral substance could be flowed through the microtube and then collected from the outlet to potentially extract biochemicals directly within a 3D tissue. Furthermore, if allowed by the rigidity of the formed 3D tissue, a dissolvable material could be used for the microtube and this would not only allow a direct delivery of substance without diffusion through a hydrogel but also potentially cells extraction from the center of a 3D tissue which would open doors to more interesting applications.

Although only spheroids were generated in this work, this platform could easily be used to perform studies on organoids since the cells seeding process through centrifugation is also applicable for organoid-derived cells. The well cavity can also be further modified through the 3D printed mold to obtain the desired organoid shape. This could be particularly useful for intestinal organoids to obtain the villi and crypts structure similar to the ones engineered by Nikolaev *et al.* and Wang *et al.*[41,44] The inner core point source delivery system of our platform would also enable lumen requiring studies such as host-pathogen interactions and soluble absorption.

While the inlet of the glass-hydrogel microtube is connected to a syringe pump to power the delivery, the outlet could be easily connected to other tissue-on-a-string units through simple tubing. The connected platforms could be other types of spheroids or organoids creating a new form of co-culture system. With simple valves and fitters, different cell culture models could be connected into a network to form a "body-on-a-string" similar to the *InVADE* platform developed by Lai *et al.* which would allow studies on complex organs dynamics. Current body-on-a-chip platforms consists mostly of 2D cell culture as their interconnection systems already makes them exceptionally intricate platforms. However, the modular property of our tissue-on-a-string platform could potentially create a system combining the benefit of the body-on-a-chip platforms and 3D cell culture models.

7. Conclusion

In this work, a 3D cell culture platform with an artificial accessible lumen was developed. It was shown that by implementing a glass-sheathed hydrogel microtube within PAAm microwell, point-source delivery to the center core of a 3D cell culture model was made possible. Not only this

allows the studies of mass transport across 3D cell culture without the need for high-end fabrication tools to create state-of-the-art controlled lumenized cultures, but it also prevents necrotic core formation for large spheroids and organoids without the need for complex vascularization. We demonstrated an application of the developed platform through studying the mass transport of a standardized molecule with controlled molecular weight and size through a 3D placental model consisting of BeWo cells. We successfully showed that higher forskolin concentration, a syncytialization inducer, reduces the transport of soluble across the placenta model. In addition, by comparing the concentration profile within the culture to a finite element model, we showed that the diffusivity within BeWo spheroid could be gradually increasing from center to edge. Although our tissue-on-a-string platform was only used for spheroids, it could be easily applied to more complex 3D cell culture such as organoids as the formation method combining microwell and centrifugation could be applied to a wide range of cell cultures.

References

(1) Jensen, C.; Teng, Y. Is It Time to Start Transitioning From 2D to 3D Cell Culture? *Front. Mol. Biosci.* **2020**, *7*.

(2) Hofer, M.; Lutolf, M. P. Engineering Organoids. *Nat. Rev. Mater.* **2021**, *6* (5), 402–420. https://doi.org/10.1038/s41578-021-00279-y.

(3) Sutherland, R. M.; Inch, W. R.; McCredie, J. A.; Kruuv, J. A Multi-Component Radiation Survival Curve Using an in Vitro Tumour Model. *Int. J. Radiat. Biol. Relat. Stud. Phys. Chem. Med.* **1970**, *18* (5), 491–495. https://doi.org/10.1080/09553007014551401.

(4) Sutherland, R. M.; McCredie, J. A.; Inch, W. R. Growth of Multicell Spheroids in Tissue Culture as a Model of Nodular Carcinomas. *J. Natl. Cancer Inst.* **1971**, *46* (1), 113–120.

(5) Kratochvil, M. J.; Seymour, A. J.; Li, T. L.; Paşca, S. P.; Kuo, C. J.; Heilshorn, S. C. Engineered Materials for Organoid Systems. *Nat. Rev. Mater.* **2019**, *4* (9), 606–622. https://doi.org/10.1038/s41578-019-0129-9.

(6) Gong, X.; Lin, C.; Cheng, J.; Su, J.; Zhao, H.; Liu, T.; Wen, X.; Zhao, P. Generation of Multicellular Tumor Spheroids with Microwell-Based Agarose Scaffolds for Drug Testing. *PLOS ONE* **2015**, *10* (6), e0130348. https://doi.org/10.1371/journal.pone.0130348.

(7) Kim, C.; Bang, J. H.; Kim, Y. E.; Lee, S. H.; Kang, J. Y. On-Chip Anticancer Drug Test of Regular Tumor Spheroids Formed in Microwells by a Distributive Microchannel Network. *Lab. Chip* **2012**, *12* (20), 4135–4142. https://doi.org/10.1039/C2LC40570A.

(8) Tung, Y.-C.; Hsiao, A. Y.; Allen, S. G.; Torisawa, Y.; Ho, M.; Takayama, S. High-Throughput 3D Spheroid Culture and Drug Testing Using a 384 Hanging Drop Array. *The Analyst* **2011**, *136* (3), 473–478. https://doi.org/10.1039/c0an00609b.

(9) Lin, R.-Z.; Lin, R.-Z.; Chang, H.-Y. Recent Advances in Three-Dimensional Multicellular Spheroid Culture for Biomedical Research. *Biotechnol. J.* **2008**, *3* (9–10), 1172–1184. https://doi.org/10.1002/biot.200700228.

(10) Lv, D.; Hu, Z.; Lu, L.; Lu, H.; Xu, X. Three-Dimensional Cell Culture: A Powerful Tool in Tumor Research and Drug Discovery. *Oncol. Lett.* **2017**, *14* (6), 6999–7010. https://doi.org/10.3892/ol.2017.7134.

(11) Zhang, B.; Li, Y.; Wang, G.; Jia, Z.; Li, H.; Peng, Q.; Gao, Y. Fabrication of Agarose Concave Petridish for 3D-Culture Microarray Method for Spheroids Formation of Hepatic Cells. *J. Mater. Sci. Mater. Med.* **2018**, *29* (5), 49. https://doi.org/10.1007/s10856-018-6058-0.

(12) Zhao, L.; Mok, S.; Moraes, C. Micropocket Hydrogel Devices for All-in-One Formation, Assembly, and Analysis of Aggregate-Based Tissues. *Biofabrication* **2019**, *11* (4), 045013. https://doi.org/10.1088/1758-5090/ab30b4.

(13) Bratt-Leal, A. M.; Nguyen, A. H.; Hammersmith, K. A.; Singh, A.; McDevitt, T. C. A Microparticle Approach to Morphogen Delivery within Pluripotent Stem Cell Aggregates. *Biomaterials* **2013**, *34* (30), 7227–7235. https://doi.org/10.1016/j.biomaterials.2013.05.079.

(14) Liao, W.; Wang, J.; Xu, J.; You, F.; Pan, M.; Xu, X.; Weng, J.; Han, X.; Li, S.; Li, Y.; Liang, K.; Peng, Q.; Gao, Y. High-Throughput Three-Dimensional Spheroid Tumor Model Using a Novel Stamp-like Tool. *J. Tissue Eng.* **2019**, *10*. https://doi.org/10.1177/2041731419889184.

(15) Brandenberg, N.; Hoehnel, S.; Kuttler, F.; Homicsko, K.; Ceroni, C.; Ringel, T.; Gjorevski, N.; Schwank, G.; Coukos, G.; Turcatti, G.; Lutolf, M. P. High-Throughput Automated Organoid Culture via Stem-Cell Aggregation in Microcavity Arrays. *Nat. Biomed. Eng.* **2020**, *4* (9), 863–874. https://doi.org/10.1038/s41551-020-0565-2.
(16) Kibschull, M. Differentiating Mouse Embryonic Stem Cells into Embryoid Bodies in AggreWell Plates. *Cold Spring Harb. Protoc.* **2017**, *2017* (6), pdb.prot094169. https://doi.org/10.1101/pdb.prot094169.
(17) Nakazawa, K.; Izumi, Y.; Fukuda, J.; Yasuda, T. Hepatocyte Spheroid Culture on a Polydimethylsiloxane Chip Having Microcavities. *J. Biomater. Sci. Polym. Ed.* **2006**, *17* (8), 859–873. https://doi.org/10.1163/156856206777996853.
(18) Goral, V. N.; Au, S. H.; Faris, R. A.; Yuen, P. K. Microstructured Multi-Well Plate for Three-Dimensional Packed Cell Seeding and Hepatocyte Cell Culture. *Biomicrofluidics* **2014**, *8* (4), 046502. https://doi.org/10.1063/1.4892978.
(19) Choi, Y. Y.; Chung, B. G.; Lee, D. H.; Khademhosseini, A.; Kim, J.-H.; Lee, S.-H. Controlled-Size Embryoid Body Formation in Concave Microwell Arrays. *Biomaterials* **2010**, *31* (15), 4296–4303. https://doi.org/10.1016/j.biomaterials.2010.01.115.
(20) Kouroupis, D.; Correa, D. Increased Mesenchymal Stem Cell Functionalization in Three-Dimensional Manufacturing Settings for Enhanced Therapeutic Applications. *Front. Bioeng. Biotechnol.* **2021**, *9*.
(21) Mukomoto, R.; Nashimoto, Y.; Terai, T.; Imaizumi, T.; Hiramoto, K.; Ino, K.; Yokokawa, R.; Miura, T.; Shiku, H. Oxygen Consumption Rate of Tumour Spheroids during Necrotic-like Core Formation. *Analyst* **2020**, *145* (19), 6342–6348. https://doi.org/10.1039/D0AN00979B.
(22) Glicklis, R.; Merchuk, J. C.; Cohen, S. Modeling Mass Transfer in Hepatocyte Spheroids via Cell Viability, Spheroid Size, and Hepatocellular Functions. *Biotechnol. Bioeng.* **2004**, *86* (6), 672–680. https://doi.org/10.1002/bit.20086.
(23) Ungrin, M. D.; Joshi, C.; Nica, A.; Bauwens, C.; Zandstra, P. W. Reproducible, Ultra High-Throughput Formation of Multicellular Organization from Single Cell Suspension-Derived Human Embryonic Stem Cell Aggregates. *PLOS ONE* **2008**, *3* (2), e1565. https://doi.org/10.1371/journal.pone.0001565.
(24) Schutgens, F.; Clevers, H. Human Organoids: Tools for Understanding Biology and Treating Diseases. *Annu. Rev. Pathol. Mech. Dis.* **2020**, *15* (1), 211–234. https://doi.org/10.1146/annurev-pathmechdis-012419-032611.
(25) Park, S. E.; Georgescu, A.; Huh, D. Organoids-on-a-Chip. *Science* **2019**, *364* (6444), 960–965. https://doi.org/10.1126/science.aaw7894.
(26) Rossi, G.; Manfrin, A.; Lutolf, M. P. Progress and Potential in Organoid Research. *Nat. Rev. Genet.* **2018**, *19* (11), 671–687. https://doi.org/10.1038/s41576-018-0051-9.
(27) Phipson, B.; Er, P. X.; Combes, A. N.; Forbes, T. A.; Howden, S. E.; Zappia, L.; Yen, H.-J.; Lawlor, K. T.; Hale, L. J.; Sun, J.; Wolvetang, E.; Takasato, M.; Oshlack, A.; Little, M. H. Evaluation of Variability in Human Kidney Organoids. *Nat. Methods* **2019**, *16* (1), 79–87. https://doi.org/10.1038/s41592-018-0253-2.
(28) de Souza, N. Organoid Variability Examined. *Nat. Methods* **2017**, *14* (7), 655–655. https://doi.org/10.1038/nmeth.4362.
(29) Gehling, K.; Parekh, S.; Schneider, F.; Kirchner, M.; Kondylis, V.; Nikopoulou, C.; Tessarz, P. RNA-Sequencing of Single Cholangiocyte-Derived Organoids Reveals High Organoid-to

Organoid Variability. *Life Sci. Alliance* **2022**, *5* (12), e202101340. https://doi.org/10.26508/lsa.202101340.

(30) Velasco, S.; Kedaigle, A. J.; Simmons, S. K.; Nash, A.; Rocha, M.; Quadrato, G.; Paulsen, B.; Nguyen, L.; Adiconis, X.; Regev, A.; Levin, J. Z.; Arlotta, P. Individual Brain Organoids Reproducibly Form Cell Diversity of the Human Cerebral Cortex. *Nature* **2019**, *570* (7762), 523–527. https://doi.org/10.1038/s41586-019-1289-x.

(31) Camp, J. G.; Badsha, F.; Florio, M.; Kanton, S.; Gerber, T.; Wilsch-Bräuninger, M.; Lewitus, E.; Sykes, A.; Hevers, W.; Lancaster, M.; Knoblich, J. A.; Lachmann, R.; Pääbo, S.; Huttner, W. B.; Treutlein, B. Human Cerebral Organoids Recapitulate Gene Expression Programs of Fetal Neocortex Development. *Proc. Natl. Acad. Sci.* **2015**, *112* (51), 15672–15677. https://doi.org/10.1073/pnas.1520760112.

(32) Krausova, M.; Korinek, V. Wnt Signaling in Adult Intestinal Stem Cells and Cancer. *Cell. Signal.* **2013**, *26*. https://doi.org/10.1016/j.cellsig.2013.11.032.

(33) Kim, G.-A.; Ginga, N. J.; Takayama, S. Integration of Sensors in Gastrointestinal Organoid Culture for Biological Analysis. *Cell. Mol. Gastroenterol. Hepatol.* **2018**, *6* (1), 123-131.e1. https://doi.org/10.1016/j.jcmgh.2018.03.002.

(34) Xia, P.-F.; Ling, H.; Foo, J. L.; Chang, M. W. Synthetic Genetic Circuits for Programmable Biological Functionalities. *Biotechnol. Adv.* **2019**, *37* (6), 107393. https://doi.org/10.1016/j.biotechadv.2019.04.015.

(35) Bashor, C. J.; Collins, J. J. Understanding Biological Regulation Through Synthetic Biology. *Annu. Rev. Biophys.* **2018**, *47* (1), 399–423. https://doi.org/10.1146/annurev-biophys-070816-033903.

(36) Zhang, F. Development of CRISPR-Cas Systems for Genome Editing and Beyond. *Q. Rev. Biophys.* **2019**, *52*, e6. https://doi.org/10.1017/S0033583519000052.

(37) Sato, T.; Vries, R. G.; Snippert, H. J.; van de Wetering, M.; Barker, N.; Stange, D. E.; van Es, J. H.; Abo, A.; Kujala, P.; Peters, P. J.; Clevers, H. Single Lgr5 Stem Cells Build Crypt-Villus Structures in Vitro without a Mesenchymal Niche. *Nature* **2009**, *459* (7244), 262–265. https://doi.org/10.1038/nature07935.

(38) Aisenbrey, E. A.; Murphy, W. L. Synthetic Alternatives to Matrigel. *Nat. Rev. Mater.* **2020**, *5* (7), 539–551. https://doi.org/10.1038/s41578-020-0199-8.

(39) Chaudhuri, O.; Cooper-White, J.; Janmey, P. A.; Mooney, D. J.; Shenoy, V. B. Effects of Extracellular Matrix Viscoelasticity on Cellular Behaviour. *Nature* **2020**, *584* (7822), 535–546. https://doi.org/10.1038/s41586-020-2612-2.

(40) Kakni, P.; Hueber, R.; Knoops, K.; López-Iglesias, C.; Truckenmüller, R.; Habibovic, P.; Giselbrecht, S. Intestinal Organoid Culture in Polymer Film-Based Microwell Arrays. *Adv. Biosyst.* **2020**, *4* (10), 2000126. https://doi.org/10.1002/adbi.202000126.

(41) Wang, Y.; Gunasekara, D. B.; Reed, M. I.; DiSalvo, M.; Bultman, S. J.; Sims, C. E.; Magness, S. T.; Allbritton, N. L. A Microengineered Collagen Scaffold for Generating a Polarized Crypt-Villus Architecture of Human Small Intestinal Epithelium. *Biomaterials* **2017**, *128*, 44–55. https://doi.org/10.1016/j.biomaterials.2017.03.005.

(42) Lai, B. F. L.; Huyer, L. D.; Lu, R. X. Z.; Drecun, S.; Radisic, M.; Zhang, B. InVADE: Integrated Vasculature for Assessing Dynamic Events. *Adv. Funct. Mater.* **2017**, *27* (46), 1703524. https://doi.org/10.1002/adfm.201703524.

(43) Rajasekar, S.; Y. Lin, D. S.; Zhang, F.; Sotra, A.; Boshart, A.; Clotet-Freixas, S.; Liu, A.; A. Hirota, J.; Ogawa, S.; Konvalinka, A.; Zhang, B. Subtractive Manufacturing with Swelling Induced Stochastic Folding of Sacrificial Materials for Fabricating Complex Perfusable Tissues in Multi-Well Plates. *Lab. Chip* **2022**, *22* (10), 1929–1942. https://doi.org/10.1039/D1LC01141C.

(44) Nikolaev, M.; Mitrofanova, O.; Broguiere, N.; Geraldo, S.; Dutta, D.; Tabata, Y.; Elci, B.; Brandenberg, N.; Kolotuev, I.; Gjorevski, N.; Clevers, H.; Lutolf, M. P. Homeostatic Mini-Intestines through Scaffold-Guided Organoid Morphogenesis. *Nature* **2020**, *585* (7826), 574–578. https://doi.org/10.1038/s41586-020-2724-8.

(45) Tse, J. R.; Engler, A. J. Preparation of Hydrogel Substrates with Tunable Mechanical Properties. *Curr. Protoc. Cell Biol.* **2010**, *Chapter 10*, Unit 10.16. https://doi.org/10.1002/0471143030.cb1016s47.

(46) Yuk, H.; Zhang, T.; Lin, S.; Parada, G. A.; Zhao, X. Tough Bonding of Hydrogels to Diverse Non-Porous Surfaces. *Nat. Mater.* **2016**, *15* (2), 190–196. https://doi.org/10.1038/nmat4463.

(47) Díaz-Bello, B.; Monroy-Romero, A. X.; Pérez-Calixto, D.; Zamarrón-Hernández, D.; Serna-Marquez, N.; Vázquez-Victorio, G.; Hautefeuille, M. Method for the Direct Fabrication of Polyacrylamide Hydrogels with Controlled Stiffness in Polystyrene Multiwell Plates for Mechanobiology Assays. *ACS Biomater. Sci. Eng.* **2019**, *5* (9), 4219–4227. https://doi.org/10.1021/acsbiomaterials.9b00988.

(48) Shoga, J. S.; Graham, B. T.; Wang, L.; Price, C. Direct Quantification of Solute Diffusivity in Agarose and Articular Cartilage Using Correlation Spectroscopy. *Ann. Biomed. Eng.* **2017**, *45* (10), 2461–2474. https://doi.org/10.1007/s10439-017-1869-6.

(49) Kandow, C. E.; Georges, P. C.; Janmey, P. A.; Beningo, K. A. Polyacrylamide Hydrogels for Cell Mechanics: Steps toward Optimization and Alternative Uses. *Methods Cell Biol.* **2007**, *83*, 29–46. https://doi.org/10.1016/S0091-679X(07)83002-0.

(50) Caliari, S. R.; Burdick, J. A. A Practical Guide to Hydrogels for Cell Culture. *Nat. Methods* **2016**, *13* (5), 405–414. https://doi.org/10.1038/nmeth.3839.

(51) Zarrintaj, P.; Manouchehri, S.; Ahmadi, Z.; Saeb, M. R.; Urbanska, A. M.; Kaplan, D. L.; Mozafari, M. Agarose-Based Biomaterials for Tissue Engineering. *Carbohydr. Polym.* **2018**, *187*, 66–84. https://doi.org/10.1016/j.carbpol.2018.01.060.

(52) *Running agarose and polyacrylamide gels | IDT*. Integrated DNA Technologies. https://www.idtdna.com/pages/education/decoded/article/running-agarose-and-polyacrylamide-gels (accessed 2022-09-09).

(53) de Vries, R.; Stell, A.; Mohammed, S.; Hermanns, C.; Martinez, A. H.; Jetten, M.; van Apeldoorn, A. Chapter 33 - Bioengineering, Biomaterials, and β-Cell Replacement Therapy. In *Transplantation, Bioengineering, and Regeneration of the Endocrine Pancreas*; Orlando, G., Piemonti, L., Ricordi, C., Stratta, R. J., Gruessner, R. W. G., Eds.; Academic Press, 2020; pp 461–486. https://doi.org/10.1016/B978-0-12-814831-0.00033-6.

(54) Chai, K. B. HYDROPHILIC POLYACRYLAMIDE GEL AND SOFT-TISSUE IMPLANTS. *Plast. Reconstr. Surg.* **2003**, *111* (7), 2497. https://doi.org/10.1097/01.PRS.0000064820.39169.F7.

(55) Singh, S. K.; Abbas, S.; Saxena, A. K.; Tiwari, S.; Sharma, L. K.; Tiwari, M. Critical Role of Three-Dimensional Tumorsphere Size on Experimental Outcome. *BioTechniques* **2020**, *69* (5), 333–338. https://doi.org/10.2144/btn-2020-0081.

(56) Kalashnikov, N.; Moraes, C. Morphodynamic Tissues via Integrated Programmable Shape Memory Actuators. *Adv. Funct. Mater.* **2019**, *29* (34), 1903327. https://doi.org/10.1002/adfm.201903327.
(57) Ryhänen, J.; Niemi, E.; Serlo, W.; Niemelä, E.; Sandvik, P.; Pernu, H.; Salo, T. Biocompatibility of Nickel-Titanium Shape Memory Metal and Its Corrosion Behavior in Human Cell Cultures. *J. Biomed. Mater. Res.* **1997**, *35* (4), 451–457. https://doi.org/10.1002/(SICI)1097-4636(19970615)35:4<451::AID-JBM5>3.0.CO;2-G.
(58) Kujala, S.; Pajala, A.; Kallioinen, M.; Pramila, A.; Tuukkanen, J.; Ryhänen, J. Biocompatibility and Strength Properties of Nitinol Shape Memory Alloy Suture in Rabbit Tendon. *Biomaterials* **2004**, *25* (2), 353–358. https://doi.org/10.1016/s0142-9612(03)00488-5.
(59) Sakaguchi, Y.; Sato, T.; Muranishi, Y.; Yutaka, Y.; Komatsu, T.; Omori, K.; Nakamura, T.; Date, H. Development of a Novel Tissue-Engineered Nitinol Frame Artificial Trachea with Native-like Physical Characteristics. *J. Thorac. Cardiovasc. Surg.* **2018**, *156* (3), 1264–1272. https://doi.org/10.1016/j.jtcvs.2018.04.073.
(60) Chen, G.; Liu, J.; Dong, Z.; Li, Y.; Zhao, Y.; Zhang, B.; Cao, J. Understanding Mechanisms of Shape Memory Function Deterioration for Nitinol Alloy during Non-Equilibrium Solidification by Electron Beam. *J. Adv. Res.* **2021**, *33*, 99–108. https://doi.org/10.1016/j.jare.2021.02.007.
(61) Heaton, S. J.; Eady, J. J.; Parker, M. L.; Gotts, K. L.; Dainty, J. R.; Fairweather-Tait, S. J.; McArdle, H. J.; Srai, K. S.; Elliott, R. M. The Use of BeWo Cells as an in Vitro Model for Placental Iron Transport. *Am. J. Physiol. - Cell Physiol.* **2008**, *295* (5), C1445–C1453. https://doi.org/10.1152/ajpcell.00286.2008.
(62) Lyden, T. W.; Ah-Kau, N. G.; Rote, N. S. Modulation of Phosphatidylserine Epitope Expression by BeWo Cells during Forskolin Treatment. *Placenta* **1993**, *14* (2), 177–186. https://doi.org/10.1016/S0143-4004(05)80259-0.
(63) Parameshwar, P. K.; Sagrillo-Fagundes, L.; Fournier, C.; Girard, S.; Vaillancourt, C.; Moraes, C. Disease-Specific Extracellular Matrix Composition Regulates Placental Trophoblast Fusion Efficiency. *Biomater. Sci.* **2021**, *9* (21), 7247–7256. https://doi.org/10.1039/D1BM00799H.
(64) Orendi, K.; Gauster, M.; Moser, G.; Meiri, H.; Huppertz, B. The Choriocarcinoma Cell Line BeWo: Syncytial Fusion and Expression of Syncytium-Specific Proteins. *Reprod. Camb. Engl.* **2010**, *140* (5), 759–766. https://doi.org/10.1530/REP-10-0221.
(65) Al-Nasiry, S.; Spitz, B.; Hanssens, M.; Luyten, C.; Pijnenborg, R. Differential Effects of Inducers of Syncytialization and Apoptosis on BeWo and JEG-3 Choriocarcinoma Cells. *Hum. Reprod.* **2006**, *21* (1), 193–201. https://doi.org/10.1093/humrep/dei272.
(66) Lee, W.; Kalashnikov, N.; Mok, S.; Halaoui, R.; Kuzmin, E.; Putnam, A. J.; Takayama, S.; Park, M.; McCaffrey, L.; Zhao, R.; Leask, R. L.; Moraes, C. Dispersible Hydrogel Force Sensors Reveal Patterns of Solid Mechanical Stress in Multicellular Spheroid Cultures. *Nat. Commun.* **2019**, *10* (1), 1–14. https://doi.org/10.1038/s41467-018-07967-4.

8. Appendix – Supplemental Materials

8.1 Dextran concentration calibration curve

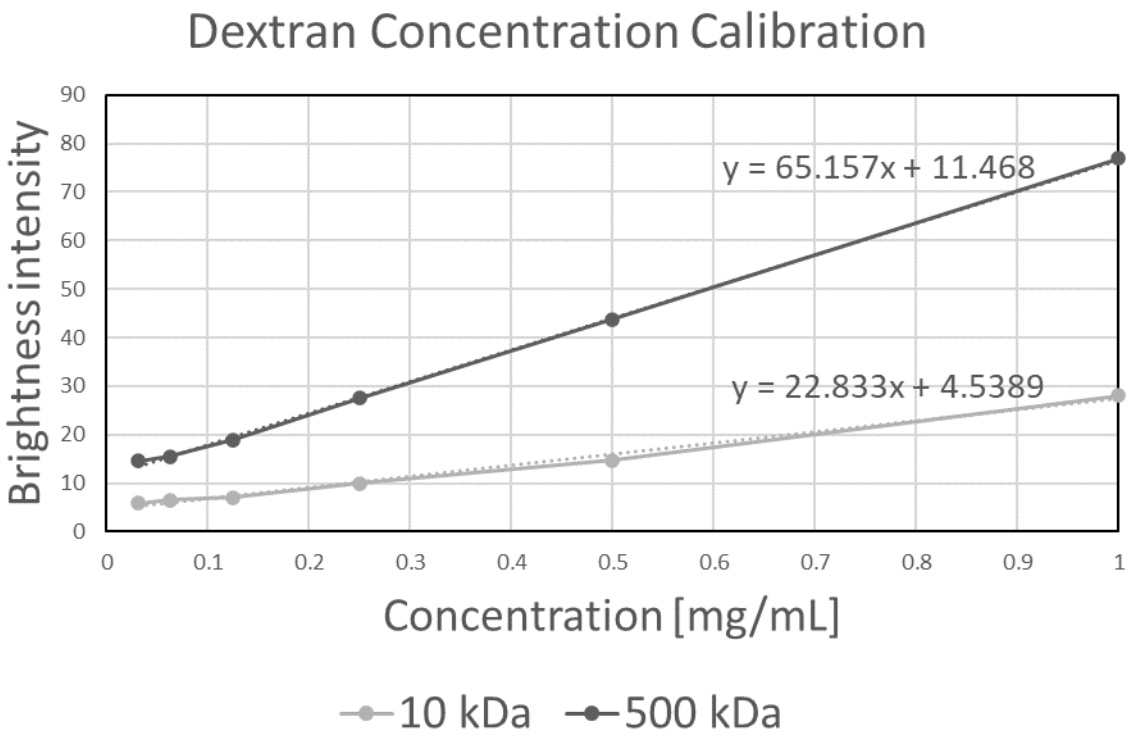

Figure 25. Dextran fluorescence intensity to concentration calibration curve.

8.2 BeWo spheroid SDC-1 staining

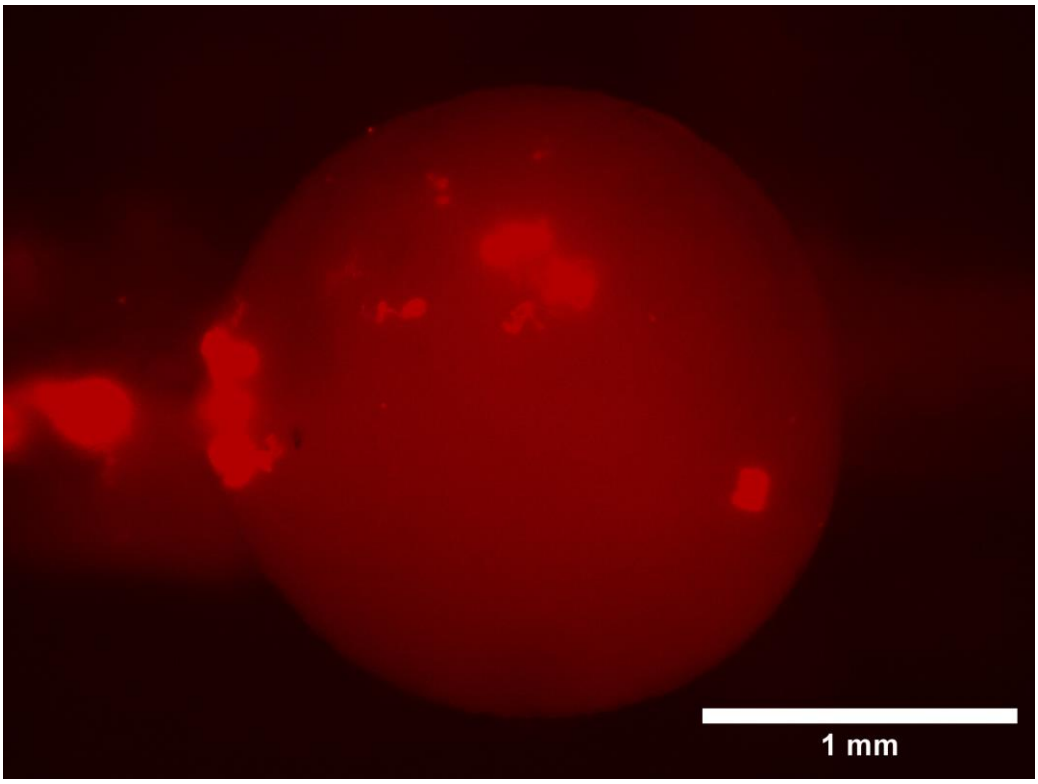

Figure 26. SDC-1 staining on BeWo spheroid.

8.3 Effect of forskolin on BeWo membrane contractility

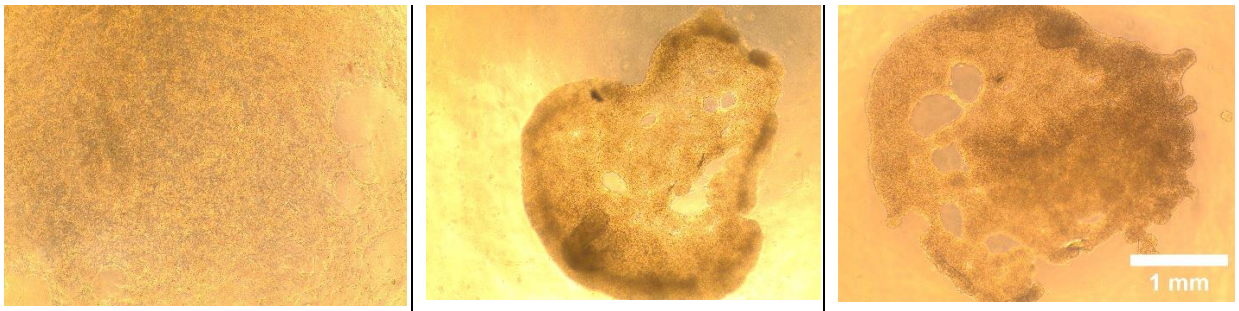

Figure 27. BeWo membrane grown on PAAm gel under treated with 50, 75 and 100 µM forskolin.

8.4 Modeled intensity curve with low imaging depth

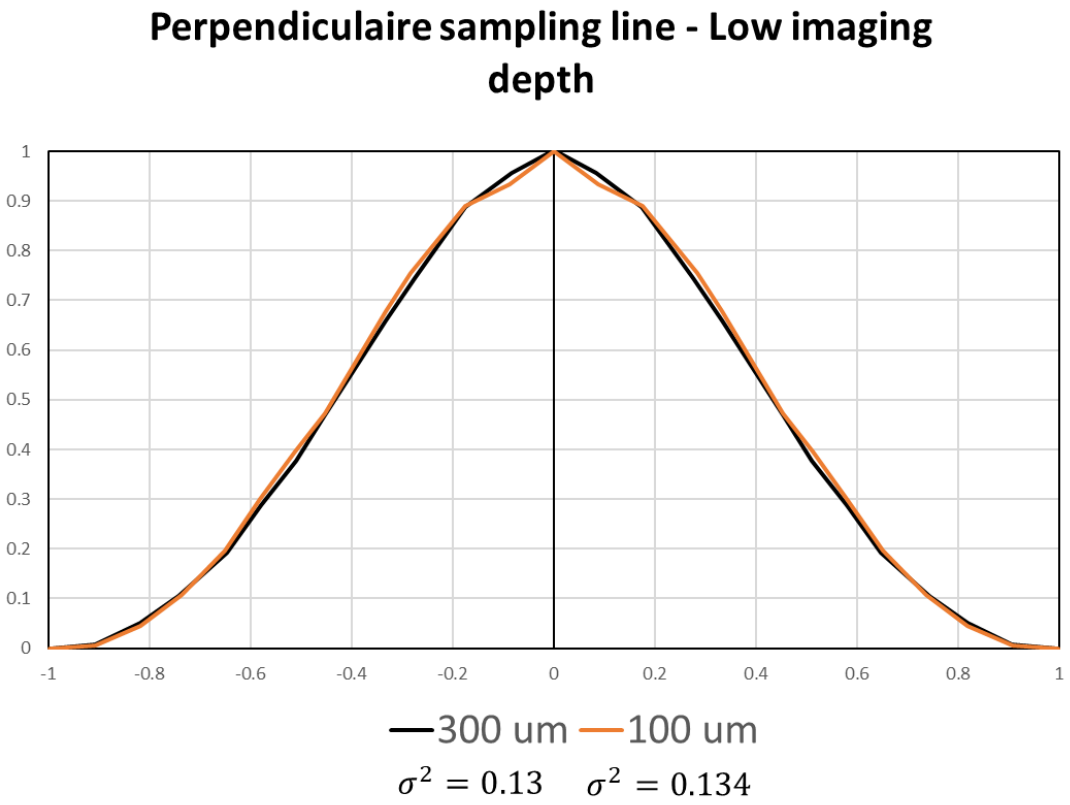

Figure 28. Modeled concentration intensity curve for perpendicular sampling line at 300 µm and 100 µm imaging depth.